INVERSE SOLUTIONS OF CONVECTIVE HEAT TRANSFER PROBLEMS

by

ARDESHIR BANGIAN TABRIZI

A dissertation submitted to the

School of Graduate Studies

Rutgers, The State University of New Jersey

In partial fulfillment of the requirements

For the degree of

Doctor of Philosophy

Graduate Program in Mechanical & Aerospace Engineering

Written under the direction of

Yogesh Jaluria

And approved by

_____

_____

_____

_____

New Brunswick, New Jersey

May, 2020

ABSTRACT OF THE DISSERTATION

Inverse Solutions of Convective Heat Transfer Problems

By ARDESHIR BANGIAN TABRIZI

Dissertation Director:

Yogesh Jaluria

Inverse problems are well known in nearly every discipline of science and engineering. In mechanical engineering, in particular, inverse heat transfer problems have always been a major focus for research and improvement. Inverse heat transfer solutions are usually needed when direct measurement of a boundary condition, commonly in the form of temperature, or a thermophysical property of a material, is not feasible. Estimating the aerodynamic heating on a reentering shuttle heat shields or approximating the temperature dependence of thermal conductivity of a cooled ingot during steel tempering are examples of inverse heat transfer applications in engineering.

A new inverse methodology to tackle the inverse heat convection problem of a wall plume is studied and presented here. A detailed study of the forward problem is developed, and the results are used to build the inverse solution methodology. Through

studying the forward problem, unique interpolating functions relating plume heat source strength and location to various flow features such as steady-state temperature on the wall downstream of the plume, are developed. These functions would form up a system of equations through which plume source strength and location are estimated. A search-based optimization method, particle swarm optimization (PSO), is used to minimize the estimation error through improving the system of equations.

In the first study, numerically simulated steady-state laminar and turbulent wall plume flows are considered. Temperature variations on the wall prove to have a unique correlation with the heat input and location of the plume. Our proposed method formulates these relations into mathematical functions for distinct locations on the wall, downstream of the plume. PSO would choose the best pair, or more, of locations on the wall to read the temperatures and form up a system of equations to solve for plume heat source strength and location. Results demonstrate high accuracy in estimating both unknowns.

The second study focuses on the transient behavior of the laminar wall plume flow. It is shown that the time it takes for the temperature, at any given location downstream of the flow, to reach a maximum across the boundary layer is related to plume heat input and location. The methodology formulates these functions and PSO would find the optimal data points on the wall to form up the system of equations. The results of this study also demonstrate high accuracy in estimating both plume strength and location.

The third study is about testing the methodology against experimental data. An experiment setup of the wall plume problem was built and temperatures on the wall downstream of the plume were measured. To test the robustness of the methodology, the

same relative functions derived in the first study are applied to the experimental data to great success. The inverse solution produces accurate estimations of the heat input and source location with the experiment data as well.

The ultimate goal of this project is to provide an inverse solution to rapidly and accurately respond in applications that include free convection heat transfer, such as overheating of electronic devices and small fires in data centers and small rooms. To that end, the proposed methodology could be considered as the first step towards a more complex and general inverse heat convection solution.

Acknowledgment

This dissertation would not have been possible without the support of many people. First and foremost, my adviser, Professor Yogesh Jaluria, for his invaluable guidance, support, and encouragement throughout my Ph.D. journey. He has been an excellent mentor, and I am forever indebted to him for all I have achieved here at Rutgers.

I would like to express my sincere appreciation to my committee members, Dr. Guo, Dr. Shan whom I have had the honor of being a student of, and Dr. Albin for providing me with valuable suggestions to improve my dissertation.

I would also like to especially thank Mr. John Petrowski, without whom my experiment setup would never have materialized. He is one of the kindest people that I have ever met. He helped me from the very first design scratch to the final stages of fabrication patiently.

There are not enough words to express my gratitude to my wife, Rahil, who always believed in me and encouraged me when I self-doubted myself. You have been the pillar of my life for the last 15 years. I love you.

Last but not least, I want to thank my parents whom I miss the most. For their continuous encouragement, support, and love. I owe everything that I have achieved in my life to them.

The bulk of content included in chapters 3, 4 and 5 was previously published in [19] and [23] .

Dedication

To my better half, Rahil.

Table of Contents

List of Figures

List of Tables

Chapter 1: Introduction

A brief introduction to inverse heat transfer problems is discussed in this chapter along with the motivation and outline of the dissertation.

1.1. Inverse Heat Transfer

Inverse problems are widely common in nearly every engineering and science branch. In mechanical engineering, inverse problems have found application in the form of inverse heat transfer problems. Inverse heat transfer in engineering applications deals with situations where direct measurement of temperature or heat input is not feasible. Finding the temperature of the center of an optic furnace, estimating the aerodynamic heating of a reentering shuttle into the atmosphere, and estimating the cooling intensity parameter of a cast slab in a cooling process are some examples of inverse heat transfer applications. In the case of the reentering shuttle, for example, the aerodynamic heating of the shuttle is so high during reentry in the atmosphere that it is impossible to put a thermocouple on the surface of the shield. So, in order to find the heat flux on the shield, thermocouples were placed beneath the hot shield surface and using inverse techniques the surface temperature was calculated.

Inverse heat transfer problems usually include either heat conduction, convection or radiation and rarely, all or two of them combined. In a forward heat transfer problem, the boundary conditions of the solution domain are known, and governing equations are solved to find the temperature and if convection is involved, fluid velocity distributions. In inverse heat transfer problems, however, temperature distribution or part of it is known whereas

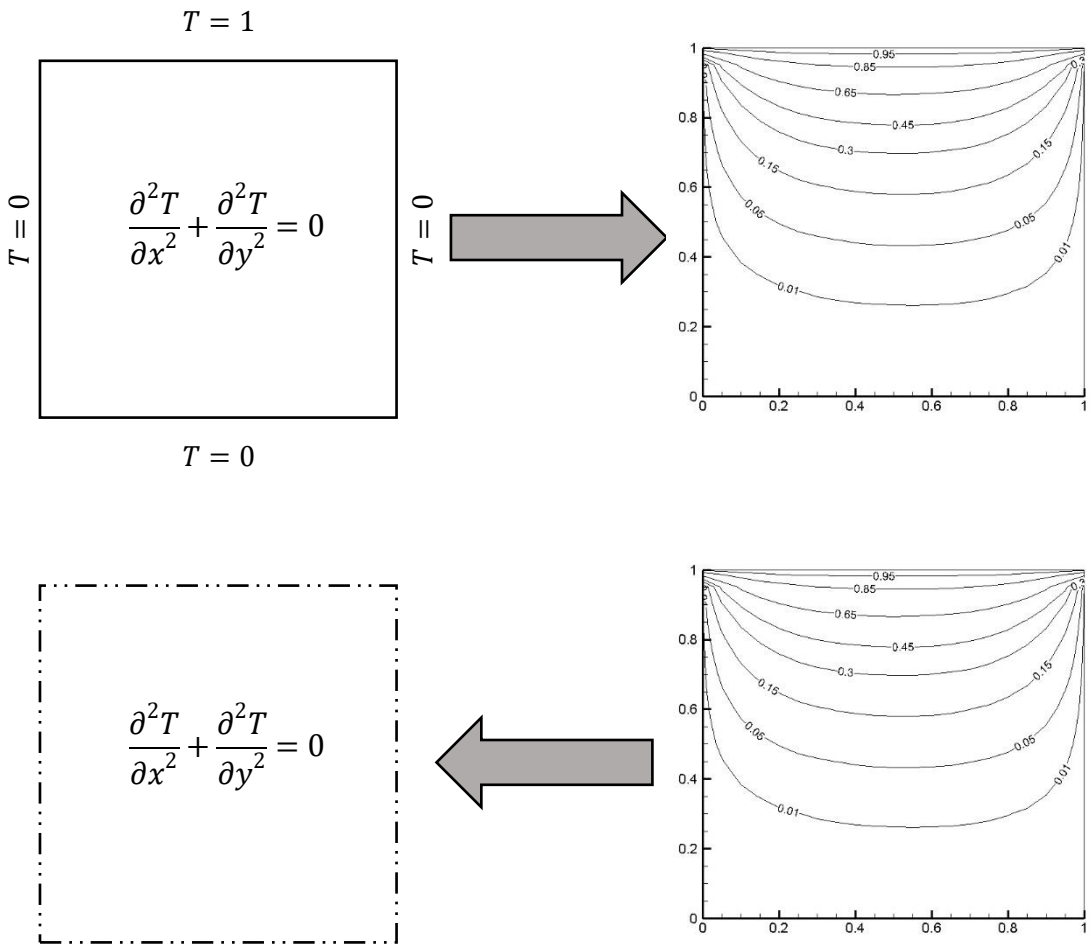

Figure 1-1- Forward and inverse heat conduction comparison

the boundary conditions are unknown. Figure 1-1 shows the basic difference between a forward and an inverse two-dimensional heat conduction problem.

While the forward heat transfer problems are considered mathematically well-posed, the inverse problems are categorized as ill-posed. For a problem to be considered well-posed, three conditions are needed. There should exist a solution, it should be unique, and it should be stable with regards to input data. If any of these conditions are not met, the problem is ill-posed. For an inverse heat transfer problem, the existence of a solution is actually a

matter of physical observation. If a certain solution domain exists, there needs to be boundary conditions. The uniqueness of the solution, however, can only be mathematically proven for a limited number of cases. It should also be noted that the inverse solutions are very sensitive to the accuracy of input, usually measured, data. Based on these observations, inverse heat transfer problems are categorized as ill-posed and as such there are no closed format solutions to them. The major challenge of an ill-posed problem is to apply certain techniques and adjustments to transform the problem into an approximate well-posed problem. These techniques usually rely heavily on numerical manipulations of the problem. With the power of computers rapidly increasing and readily available, the inverse heat transfer solutions have found momentum in the past three decades.

The most common methods to tackle the inverse heat transfer problems are the iterative approaches. These methods utilize an initial guess for the unknown parameter and then solve the domain and compare the results with the given data. These methods would adjust and improve the initial guess according to the difference between the given data and the solved domain and continue this iterative process until an acceptable accuracy is achieved. Methods such as Levenberg-Marquardt and conjugate gradients fall into the classification of the iterative methods. The iterative methods are considered as a relatively reliable and accurate approach, especially for inverse heat conduction problems. Inverse heat convection, on the other hand, introduces an obstacle in the form of nonlinear forward PDEs. This nonlinearity combined with the ill-posed nature of the inverse problem has introduced new challenges.

1.2. Motivation

A major setback for iterative methods is the time it takes to converge on the solution. Due to the nature of these methods, the entire domain needs to be solved again for each new problem even if other parameters, such as geometry and working fluid, remain the same. There are applications, such as small fires, that time is of the essence and a fast, reliable solution is desired. In addition, iterative methods usually assume that the forward data is available for the entire solution domain and so the optimum datum point can be found anywhere in the domain, however in application that is not the case. In many applications, the available data is limited to certain parts or locations in the geometry which adds another layer of difficulty to the already complex problem.

The purpose of this study is proposing an approach that would take application limitation into account and provide a reliable and prompt solution. A very common free convection flow in the form of wall plume is studied numerically in both laminar and turbulent regimes. Both steady-state and transient temperature trends are then used to build an algorithm that is capable of providing inverse solutions with the absolute minimum input, within the acceptable estimation error range, instantly. In order to validate the robustness of the algorithm, an experimental setup was built and used to gather data. The present algorithm provided inverse solutions within an acceptable range for the experimental data as well as numerical data.

1.3. Thesis Outline

In this chapter, a brief overview of the inverse problems along with their applications and limitations was provided. In Chapter 2, related research on both the forward and inverse

problem is introduced. In Chapter 3, the inverse methodology and the optimization algorithm are discussed. Chapter 4 introduces the basics of the forward laminar problem and then discusses the solution to the inverse heat convection problem using steady-state temperature. Chapters 5 continues the laminar flow analysis and expands on the transient data and its application in solving inverse heat convection. Chapter 6 covers the turbulent free convection flow and the inverse problem using steady-state temperatures. Chapter 7 describes the experimental setup and results. A conclusion and summary of the thesis are presented in Chapter 8.

Chapter 2: Literature Review

When the direct measurement of boundary or initial conditions, such as temperature or heat flux input of a thermal system is not accessible, inverse heat transfer methods are used to estimate them. While the forward problems often use the boundary and initial conditions to solve for the temperature and velocity distributions across the solution domain, inverse heat transfer problems approximate the unknown boundary conditions using the available data, usually in the form of temperature measurements at certain locations throughout the solution domain. Based on the definition by Hadamard [1], the inverse heat transfer problem is mathematically ill-posed [2]. While the forward heat problem has diffusion terms and can smooth the effect of error in boundary conditions, the inverse problem would amplify the errors of temperature measurements and lead to unacceptable results [2-4]. Being ill-posed also means that different inputs may lead to the same results thus making it more difficult to obtain a unique solution. Various methods and approaches have been studied over the years to overcome these challenges especially finding ways to limit the error amplification. Tikhonov [5], Alifanov [6-8] and Beck [2, 9] pioneered regularization and function estimation methods to approach the inverse heat transfer problems. These methods are used to reformulate the ill-posed inverse problem into an approximate well-posed one.

Most of the existing methods are developed to tackle inverse heat conduction problems (IHCP) [2, 6, 9-11]. Heat conduction has a linear forward problem and is very common in various thermal systems, so it attracted a lot of research. Inverse heat convection, on the

other hand, has a system of nonlinear governing equations. The more complicated forward problem means that many of the inverse methods that were developed for the IHCPs either needed modifications or could not be used in inverse convection studies. Huang and Ozisik [12] solved the wall heat flux in a fully developed channel flow using the temperature readings from inside the channel by applying both regular and modified conjugate gradient methods. Liu and Ozisik [13] used the same methods to find a time-varying heat flux on a wall in a fully developed turbulent channel flow. Hsu et al. [14] found both the inlet temperature and wall heat flux in a steady laminar flow in a circular duct. Knight et al. [15] estimated the temperature and velocity of a jet in a crosswind using an iterative method based on experimental and numerical data. VanderVeer and Jaluria [16] solved for strength and location of a plume in a crosswind by applying a predictor-corrector method on both numerical and experimental data using a proposed search shape. They concluded that the error can be reduced by increasing the number of measuring points. VanderVeer and Jaluria [17] optimized the number of measuring points in the search shape using Genetic algorithm. They then tested their optimized search shape on a jet in a crossflow to find the temperature and location of the jet with reasonable results [18]. Recently, Bangian-Tabrizi and Jaluria [19] used interpolative equations to relate steady-state temperature at any location downstream of a wall plume to plume strength and location. They then used the PSO optimization technique to find sensor locations on the wall and solved the system of equations consisted of each sensor`s respective interpolative equation, to solve for the plume strength and location. Na et al. [11] solved for heat transfer coefficient in a one-dimensional heat transfer problem of a cooling body using a variation of PSO called

Quantum-behaved PSO (QPSO). A summary of the recent applications and ongoing researches of inverse heat transfer in the human body is provided by Scott [20].

While the main focus of both forward and inverse heat convection problems is on studying the steady-state problems, there are attempts at solving transient problems as well. Prud'homme et al. [21] approximated a time-varying heat flux boundary condition with a single temperature sensor. They concluded that as the Rayleigh number increases the sensor needs to get closer to the source. Park and Chung [22] studied the inverse natural convection in a two-dimensional cavity to find a time-varying heat source without applying any simplifications on the Boussinesq equation. They found that a combination of modified and regular conjugate gradient methods yields the best result for their problem. Bangian-Tabrizi and Jaluria [23] used the time it takes for the leading edge to reach downstream of a wall plume to solve the inverse heat convection problem. They found that the time at which the maximum temperature across the boundary layer is the highest has a unique correlation with the plume heat input and location.

One of the fundamental flows studied in heat and mass transfer is the natural convection flow generated adjacent to a semi-infinite vertical plate with either constant temperature or heat flux boundary condition [24-26]. Ostrach [27] used a similarity solution approach to solve the steady-state, fully developed boundary flow next to an isothermal vertical flat plate. He then solved the resulting system of ODEs with numerical methods. His results were in good agreement with the experimental results of Schmidt and Beckmann [28]. Schmidt and Beckmann provided a complete theoretical and experimental study of the free convection of air adjacent to a vertical flat plate. Eckert [29] expanded Schmidt and Beckmann's experiments while Schuh [30] solved the problem for different Prandtl

numbers. Gregg and Sparrow [31] studied the laminar convection flow next to an isoflux wall.

On the transient side of the problem, Siegel [32] used Karman-Pohlhausen integral approximation method to analyze the transient natural convection flow next to a vertical flat plate. Hellums and Churchill [33] studied both transient and steady-state natural convection flow over an isothermal vertical plate. They solved the boundary layer equations numerically and verified their steady-state solution with Ostrach. They plotted the temperature and velocity profiles across the boundary layer as well as the heat convection coefficient on the wall against Ostrach similarity solution variables and showed that a similarity solution for the transient laminar problem is possible. Harris et al. [34] presented an analytical solution for the transient convection flow past a vertical flat plate, with an already fully developed steady-state flow, subjected to a sudden surface temperature change using a similarity solution approach. Maranzana et al. [35] focused on experimental data for free convection heat transfer coefficient on a flat wall.

The turbulent free convection boundary layer has also attracted research interest. Eckert and Jackson [36] used Karman integral method to model a steady-state turbulent free convection boundary layer next to a vertical plate. Cheesewright [37] then compared his experimental data against Eckert and Jackson model and showed that although the heat transfer coefficient and rate are very similar, Eckert model predicted a thicker boundary layer than the experiment. Tsunji and Nagano [38] experimental data also matched those of Cheesewright. George and Capp [39] proposed a theory to model the flow using scaling arguments. Their theoretical results matched the experimental data better than those of Eckert and Jackson. To and Humphery [40] numerically studied the turbulent free

convection flow next to a heated wall using $k-\varepsilon$ method. Their results were in good agreement with experimental data such as Cheesewright's. Nakao et al. [41] used large eddy simulation technique to model the same problem to study heat transfer rate and friction velocity. Their method yielded comparable results to experimental data of studies before them. Turbulent natural convection flow in a cavity was studied by Rundle and Lightstone [42] to validate different turbulence models for other CFD applications.

In order to fully comprehend the aspects of flow development and behavior, more detailed researches were conducted. In the very beginning phases of transient natural heat convection, heat transfer from the wall to its surrounding ambient fluid is a one-dimensional conduction process. Gradually adjacent fluid motion begins and the bulk of heated fluid starts to rise next to the wall and the problem shifts from a one-dimensional conduction from a semi-infinite medium to a two-dimensional convection [43]. The effect of this rising bulk of heated fluid is called the leading-edge effect. Sugawara and Michiyoshi [44] presented a numerical solution for the flow past an isothermal semi-infinite wall. They broke the problem into two parts. In the first part, they solved the governing equations without the convective terms to capture the initial heat conduction phase and then used this solution in the second part with full governing equations and continued the solution to steady-state. They concluded that at least for air, the conduction only phase lasts very briefly. Ahmadi and Bahrami [45] investigated the transient natural convection flow next to an isoflux wall with asymptotic methods, dividing the flow into short-time and steady-states asymptotes, and covered the full duration time of the flow.

Schetz and Eichhorn [46] solved the initial one-dimensional conduction phase using Laplace transforms for different surface temperature and flux boundary conditions. Menold

and Yang [47], Rao [48] and Miyamoto [49] all studied the one-dimensional conduction phase for different boundary conditions and fluid properties. Illingworth [50] was one of the pioneers to study the leading edge effects. Goldstein and Briggs [51] presented an analytical study of the leading edge propagation rate downstream of the flow. The leading-edge effect was treated as a wave that propagates downstream towards the one-dimensional conduction region. Heat transfer in any location on the wall that the leading edge has passed from then turns into a two-dimensional convection. They reported a closed format formula to estimate the propagation rate. Gebhart and Dring [52], Mollendorf and Gebhart [53] and Mahajang and Gebhart [54] also studied the propagation rate of the leading edge effect. Patterson et al. [55] studied the leading edge effect propagation rate using stability analysis.

One of the more interesting flows that fall under the natural convection flow adjacent to a vertical plate category is the wall plume. Wall plumes are plane flows caused by a line source, or just a point source in 2D, on a wall. Like any other buoyancy induced flow, the source heats up a bulk of fluid next to the wall and causes it to ascend and create a flow. An example would be the flow caused by a row of electronic devices on a wall in a data center. The main difference between the classic natural convection flow and the wall plume is that the surface of the wall is assumed adiabatic anywhere but on the source and so the surface does not exchange energy with the rising fluid and so the thermal energy of the fluid diffuses into the ambient fluid [43]. Transient flow behavior and temperature variation of free and wall plums have been subject to researches.

Fujii [56] presented a thorough study on free plums over both a line and a point source. He offered a closed-form boundary layer solution as well as numerical solutions for various Prandtl numbers. Gebhart et al. [57] presented a similarity solution method with

appropriate boundary conditions for free plume over a line source problem. Zimin and Lyakhov [58] studied the laminar, incompressible wall plume caused by a line source. They used the similarity solution technique to reduce the boundary layer equations to a system of ODEs and solved them numerically for water (Pr = 7). They verified their results with experimental data. Jaluria [59] discussed the effects of mixed convection on a wall plume with a finite dimension source. He found that after a certain point downstream, the flow patterns closely follow those of a wall plume with a line source reported by Jaluria and Gebhart [60]. They provided numerical results for different Prandtl numbers in the range of 0.01 to 100.

Chapter 3: Inverse Methodology

In this chapter, our proposed inverse methodology is discussed. Like every other inverse solution, this methodology relies on optimization to converge on the best estimation. A brief introduction to the optimization method used in the proposed methodology is also provided.

3.1. Methodology

The method described in this study tries to accurately solve the inverse wall plume free convection problem with different input data. The method was first developed to work with steady-state temperature data on the wall downstream of the plume source. The only information a prior is the temperature of the ambient fluid, in this case, air, next to the wall. Thus, plume location (l) and its strength, whether it's constant temperature or heat flux boundary condition, are unknown. Here, the strength of the plume source is denoted by Grashof (Gr) number. A detailed description of the forward problem is provided in the following chapters. The plume source is not a line on the wall but rather has a finite length to model the practical applications with a better approximation.

This method focuses on using the limited data available, for example, the temperature of any point on the wall, to solve for the unknown plume features. A more detailed study of these relations, discussed in the following chapters, shows that there is indeed an interpolative relation between the temperature and the plume strength and location, generally in the following form:

$$T = f(l, Gr) \tag{3-1}$$

where f is a unique function that is calculated at any point downstream of the plume, Gr is the Grashof number and l is the distance of the mid-length of the finite source to the bottom of the plate. After determining the function of equation (3-1) for all possible locations downstream of the plume, if the temperature at any given two points is known, in theory, a system of two equations can be solved to determine Gr and l.

$$\begin{cases} T_1 = f_1(l, Gr) \\ T_2 = f_2(l, Gr) \end{cases} \Longrightarrow (Gr, l) \tag{3-2}$$

It should be noted that two is the minimum number of data points needed to solve for the unknown features in the system of equations (3-2). A part of this study is dedicated to the effects of increasing the number of data points on the accuracy of the estimations. With the given information above, the question is what are the best data points?

In order to answer that question, we need to use an optimization algorithm to specify the best two points that yield the best estimation of the plume source strength and location. Most of the current inverse solution methods apply optimization in their regularization process to improve the accuracy and rate of convergence. Colaco et al. [61] provided a detailed study of inverse heat transfer problems and different optimization methods. Common iterative inverse solutions rely on optimization to minimize a pre-defined objective function, usually absolute or square estimation error, in each consecutive iterations. Deterministic and stochastic optimization techniques have been used to minimize the objective function [4, 61]. Deterministic methods rely heavily on mathematical formulations e.g. as gradients of the objective function in order to converge on the optimum point over a number of iterations. Some of the deterministic methods that

have been used in inverse heat transfer problems are steepest descent, conjugate gradient, Newton-Raphson and Levenberg-Marquardt methods [61]. As opposed to the heavy mathematics focused deterministic methods, stochastic and evolutionary optimization methods tend to minimize the objective function using algorithms inspired by natural phenomena. Genetic algorithm, differential evolution, particle swarm, and simulated annealing are a few of the stochastic methods used in inverse heat transfer problems [61].

3.2. Particle Swarm Optimization (PSO)

In this thesis, Particle Swarm Optimization or PSO was used due to simple implementation and fewer hyperparameters. PSO is a metaheuristic search-based method that was inspired by the behavior of a flock of birds or a school of fish searching for food [62]. It was first introduced by Eberhart and Kennedy [63] to optimize continues non-linear functions. Since its introduction, PSO has been a subject of interest and many modifications have been introduced through the years to improve the algorithm. Bonyadi and Michalewicz [64] and Zhang and Wang [65] recently published comprehensive reviews on different aspects, approaches, and applications of PSO.

In order to solve a problem, an initial and usually random set of candidate solutions, or simply particles, are selected. These particles move around in the search-space under the influence of their own personal search history as well as the swarm's collective search history. This way, those particles that are on the better track can guide the rest of the swarm to the best position in the search space. This iterative process continues until the accuracy criteria of the problem are met or a certain number of iterations have passed [65]. In each iteration, the position and velocity of each particle are updated by:

$$V^{i+1} = \xi \cdot V^i + C_1 \cdot \gamma_1 \cdot \left(P_{Best} - P^i\right) + C_2 \cdot \gamma_2 \cdot \left(G_{Best} - P^i\right) \quad (3\text{-}3)$$

$$P^{i+1} = P^i + V^{i+1} \quad (3\text{-}4)$$

where P is particle position and V is the velocity or particle path. ξ is the inertia weight and shows how much the previous velocity is influencing the current one. C_1 and C_2 are cognitive and social factors respectively controlling the influence of a particle's personal best, P_{Best}, as well as the global best, G_{Best}, on the velocity. Finally, γ_1 and γ_2 are randomly generated numbers in the range of [0,1] in each iteration. Typical coefficient values used in (3-3 are gathered in Table 3-1. For our study, 50 to 100 particles were randomly selected to populate the initial phase. Both P and V are vectors with a dimension equal to the number of data points used. Figure 3-1 shows the algorithm at work.

The inverse method used in this study can be formulated as an optimization problem with the objective function, the estimation error of location and strength estimation, which should be minimized. Such an objective function is formulated as:

$$ObjectiveFunction = \sum_{i=1}^{N} \left(w_1 \left|\frac{Gr_{est-i} - Gr_i}{Gr_i}\right| + w_2 \left|\frac{l_{est-i} - l_i}{l_i}\right|\right) \Big/ N \quad (3\text{-}5)$$

where w_1 and w_2 are weighting factors and N is the number of particles used to populate the search domain. This objective function was defined as the summation of estimation errors of source and location. Weighting factors were added so that objective function could be modified to focus more on one of the errors if needed. There were many ways to approach the objective function including the least-squares method. Here, for the sake of simplicity, the absolute error values were chosen.

Table 3-1- Typical coefficients used in equation (3-3)

ξ	C_1	C_2
0.55~0.85	2	2

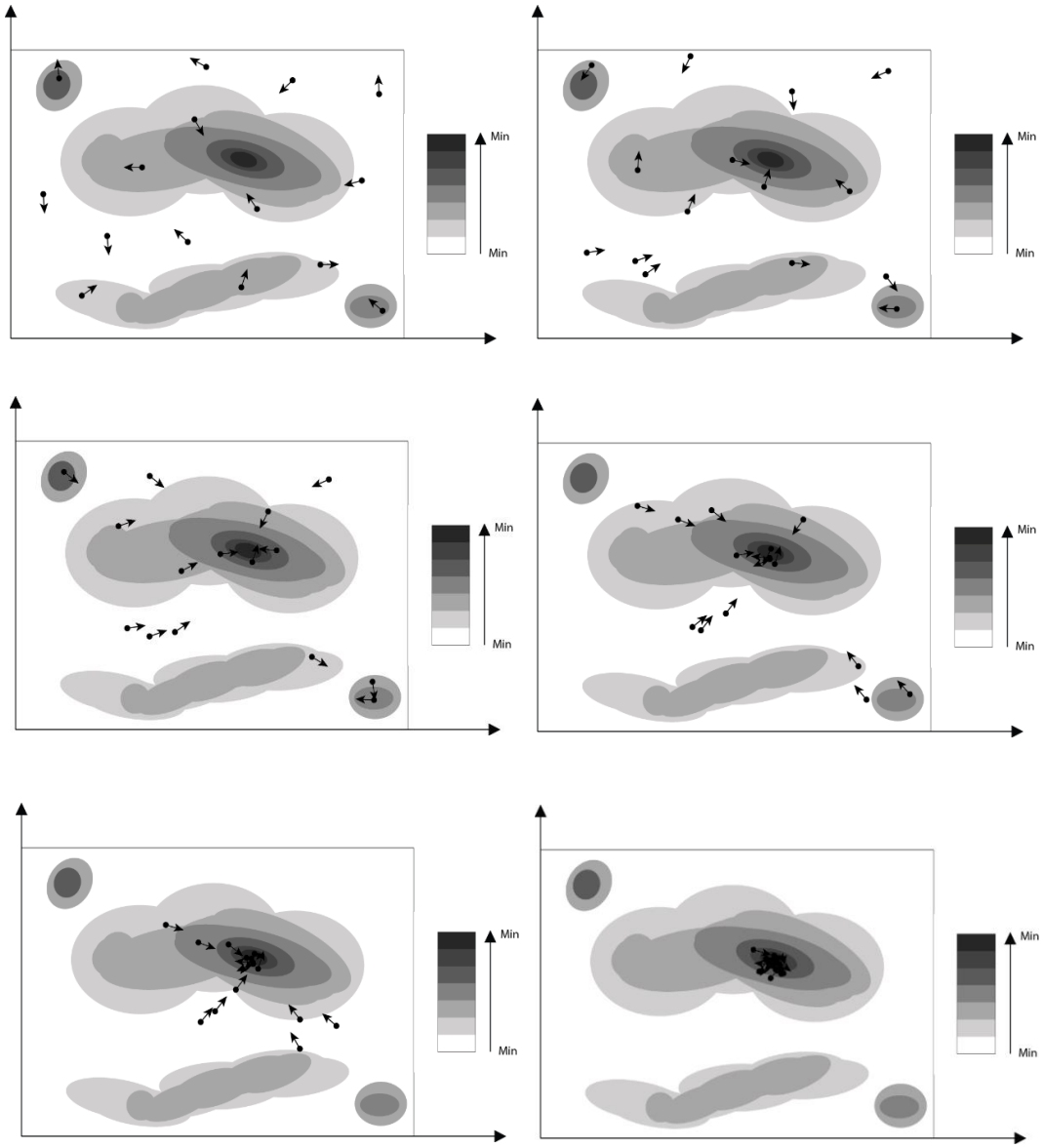

Figure 3-1- PSO convergence

Some constraints were also applied. The upper half of the plate was divided into discrete points or locations, and PSO was then bound to select particles from these points only. Also, a selected pair of locations could not have a distance smaller than 5 divisions in between. Each particle's individual best position as well as the swarm's best position is found using the objective function and is then used to update equations (3-3) and (3-4).

3.3. Conclusion

The general inverse methodology was presented in this chapter. The main goal of this study is to find interpolative functions between different flow characteristics at locations downstream of the plume, such as steady-state temperature on the wall surface, and the plume heat input and location. If these equations are unique for different locations, then they can be used to solve for the unknown plume boundary conditions. However, although all such equations would provide an estimate for the said unknowns, not all of these estimations would be in an acceptable error range. In order to find the best equation an optimization algorithm called PSO is used. PSO is a search-based optimization method that sweeps the search domain to find the optimum equations.

Chapter 4: Inverse solution – Using Steady-State Data

In this chapter, an inverse solution to the wall plume problem using relations between the steady-state temperatures on the plate and the location and strength of the plume is studied.

4.1. Physics of the Forward Problem

In order to model a transient wall plume, a laminar natural convection two-dimensional flow is presented here. Buoyancy forces are induced by a 2D heat source on a flat wall. The surrounding fluid, air, with Prandtl number Pr = 0.712, is initially at rest with temperature T_0^* when a step change in heat input is applied to the source area of the wall. Figure 4-1 showcases the geometry of the problem. L is the height of the plate and l the distance between the leading edge to the center of the heat source. For the wall plume problem considered, the following non-dimensionalizion are used. All dimensional parameters are indicated with a superscript star. A complete list of all the parameters used in this article is presented in the nomenclature.

$$t = \frac{t^* \alpha}{L^2}, \qquad x = \frac{x^*}{L}, \qquad y = \frac{y^*}{L}$$
$$l = \frac{l^*}{L}, \qquad u = \frac{u^* L}{\alpha}, \qquad T = \frac{T^* - T_0^*}{\Delta T} \tag{4-1}$$

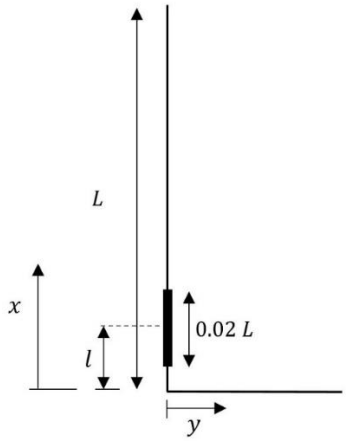

Figure 4-1- Problem geometry: L is the length of the plate and x the distance from the leading edge to the center of the source.

The Boussinesq approximation was used to model the buoyancy effects in the energy equation. Full Navier-Stokes and energy equations, written in stream function and vorticity formulation, are given in non-dimensional form by equations (4-2) to (4-4). In these equations, the x-direction is parallel to the wall and y is normal to it.

$$\frac{D\omega}{Dt} = Pr.\nabla^2\omega + Gr\,\mathrm{Pr}^2\frac{\partial T}{\partial y} \tag{4-2}$$

$$\frac{DT}{Dt} = Pr.\nabla^2 T \tag{4-3}$$

$$\nabla^2\psi = -\omega \tag{4-4}$$

where ω is vorticity, ψ is stream function, $Gr = \beta g \Delta T L^3/\nu^2$ is Grashof number and $\mathrm{Pr} = \nu/\alpha$ is the Prandtl number. The velocity components satisfy no-slip conditions on the plate. An adiabatic condition is assumed on the entire wall except for the finite height over which the heat input is given. The heat source is a portion of the wall with a fixed length (0.02L). On this finite length, the boundary condition is taken as $T^* = T_1^*$ for isothermal cases and $q''^* = q_0''^*$ for isoflux cases. For the isoflux boundary condition,

however, due to lack of a characteristic constant temperature on the boundary, a suitable definition of temperature difference is $\Delta T = q_0''^* \cdot L/k$, where k is thermal conductivity. Equations (4-2), (4-3) and (4-4) were solved in a square region with height L. The wall is treated as adiabatic everywhere except for the source region. Flow opening conditions are applied to the top and far-right boundaries. The bottom boundary has adiabatic treatment for energy equation and no-slip condition for momentum to model a typical corner flow frequently seen in electronic heating and small fires.

Both transient and steady-state results are tested against the numerically obtained boundary layer results of Churchill [33] and Ostrach [27]. To validate results, the solution domain was changed to a rectangle with a large enough height so that the boundary layer assumptions are valid. A wall with a constant temperature condition is taken on the left boundary. The bottom boundary is treated as an adiabatic with a slip condition wall. These conditions are applied to better simulate the boundary layer flow. Figure 4-2 shows both steady-state and transient temperature profiles adjacent to the wall. Here, local Grashof number is defined as $Gr_x = \beta g \Delta T x^{*3}/\nu^2$.

Based on the trends that temperature on different locations along the plate followed, several observations were made. Figure 4-3 shows the temperature variation with respect to source location, l, and heat input, given by Gr, at three different sensor locations on the plate for the forward problem.

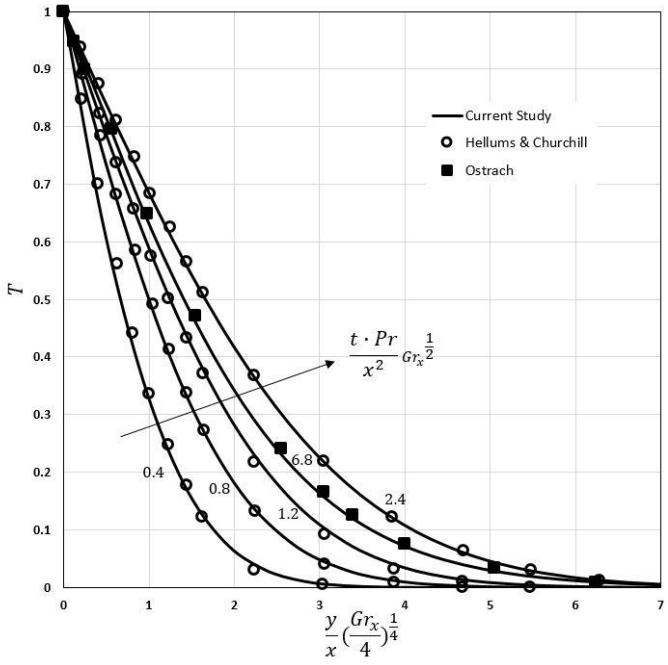

Figure 4-2- Variation of transient temperature across the boundary layer.

A series of functions, such as power-law, polynomial and exponential functions, were considered to capture the nature of these trends. One such function is the equation:

$$T \times \Delta T = a_1 Gr^{a_2} \cdot e^{[a_3 Gr^{a_4} \cdot l^{a_5}]} \quad (4\text{-}5)$$

where a_1 to a_5 are coefficients calculated at any point using nonlinear regression methods, Gr is the Grashof number and l is the distance of the mid-length of the finite source to the bottom of the plate. Polynomial part of this equation is to capture the Gr effect on the temperature trend shown in Figures 4-3a and c, while the exponential part models the source location effect, better shown in Figures 4-3b and d. In order to find these coefficients, a group of cases was chosen to be the training data set. This same data set is then later used to train the PSO algorithm. The other group of data cases is referred to as the testing data set.

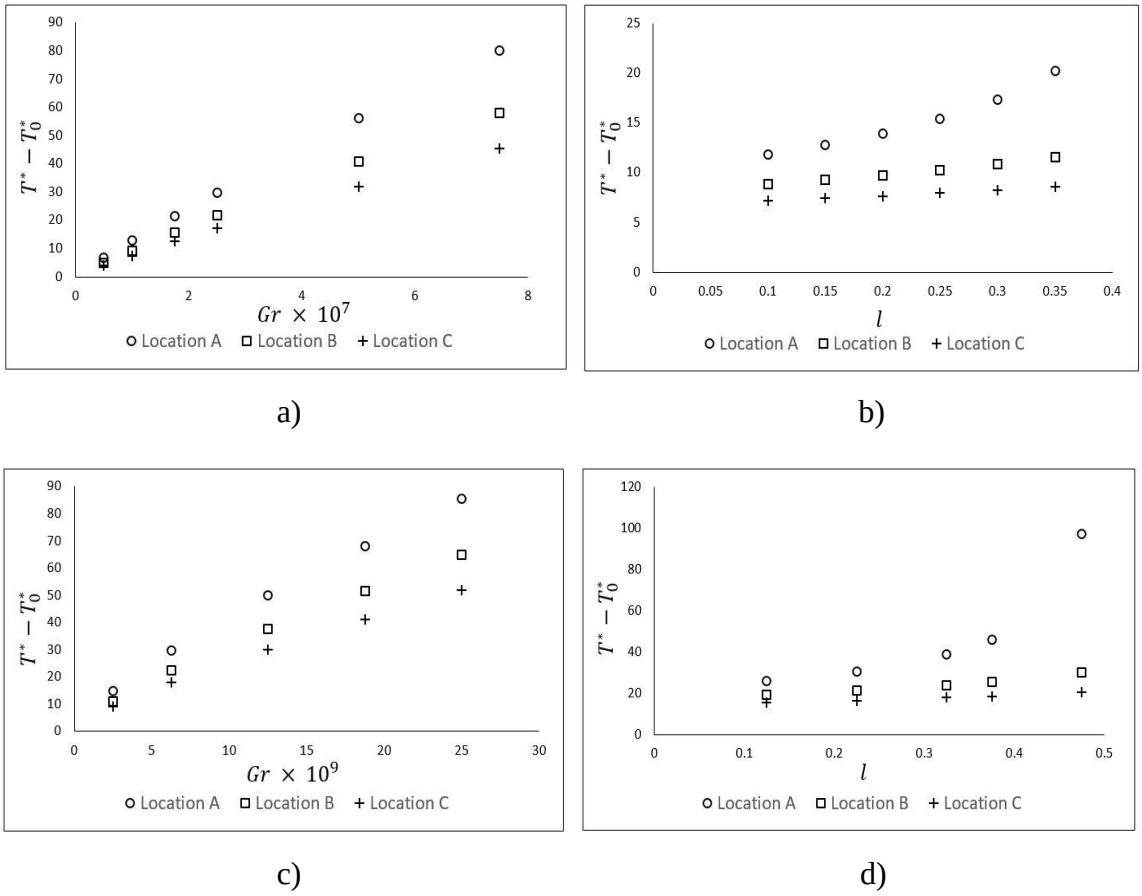

Figure 4-3- Variation of temperature with respect to (a) isothermal source strength, (b) isothermal source location, (c) isoflux source location and (d) isoflux source strength – locations A, B and C represent 0.5L, 0.75L and L on the wall

Table 4-1 showcases typical coefficients for three different locations on the plate as well as their coefficient of determination or simply R^2 values for isothermal source cases. It should be noted that these coefficients are different for isoflux sources. After determining the coefficients of equation (4-5) for all possible locations, the PSO algorithm is used to find the best two locations to use as data points or sensors.

Table 4-1- Nonlinear Regression Coefficients for Sample Locations

Location	$a_1 \times 10^{-6}$	a_2	a_3	a_4	a_5	R^2
0.5 L	4.30	0.91	2.31	0.029	1.77	0.99
0.75 L	3.14	0.91	0.65	0.043	1.31	0.99
L	3.03	0.90	0.28	0.063	1.09	0.99

4.2. Results

Three different types of problems were studied: unknown source strength, unknown source location and finally unknown source strength and location. Both isothermal and isoflux sources were studied in each problem. Forward problem temperature data with different combinations of l and Gr were used to train the optimization method. This data set was used to find the coefficients a_1 to a_5 for locations on the upper half of the plate. PSO algorithm then utilized these coefficients to find the best location, for single unknown problems, or a pair of locations for the full inverse problem to put the sensors. Due to the method's stochastic nature, the algorithm was applied a number of times with random initial swarm particles and it was observed that the presented sensor locations were the most frequent result and had the least objective function value in comparison with other outcomes of the method. The objective function definition given in equation (3-5) was simplified for single unknown problems. Table 4-2 and 4-3 showcase the different Gr and l combinations used for this study. Three type of problems were studied. Plume strength unknown, plume location unknown and finally both strength and location unknown.

Table 4-2- Gr and l Values for Isothermal Studied Cases

Case	Gr × 10^7	l	Case	Gr × 10^7	l	Case	Gr × 10^7	l
1	0.5	0.15	6	1	0.35	11	2.5	0.3
2	0.5	0.25	7	1.75	0.125	12	5	0.1
3	0.5	0.35	8	1.75	0.225	13	5	0.15
4	1	0.15	9	2.5	0.1	14	5	0.2
5	1	0.25	10	2.5	0.2	15	5	0.3

Table 4-3- Gr and l Values for isoflux Studied Cases

Case	Gr × 10^9	l	Case	Gr × 10^9	l	Case	Gr × 10^9	l
1	5	0.125	6	15	0.175	11	15	0.425
2	5	0.225	7	15	0.225	12	32.8	0.175
3	5	0.375	8	15	0.275	13	32.8	0.325
4	5	0.475	9	15	0.325			
5	15	0.125	10	15	0.375			

4.2.1 Type I: Unknown source strength

In this problem, it was assumed that source location is known. With this assumption, only one equation is needed to estimate the strength. PSO was used to find the location that would predict the source strength with the least error for all training cases. Here, each particle represents a location on the upper half of the plate. Equation (4-6) shows the simplified objective function for this problem. As mentioned earlier Gr represents source strength.

$$ObjectiveFunction = \sum_{i=1}^{N} \left| \frac{Gr_{est-i} - Gr_i}{Gr_i} \right| \Big/ N \tag{4-6}$$

Table 4-4 shows the optimum particle and its corresponding location on the plate for isothermal and isoflux source types. In order to check robustness and validity of the method, testing data cases which were not used in finding coefficients a_1 to a_5 or training process, were used. Figure 4-4 and 4-5 demonstrate the Gr estimation error for the testing

data set. Overall, the presented equation performs well in estimating the Gr in both isothermal and isoflux scenarios. Equation (4-5), along with coefficients provided in Table 4-1, suggests that temperature shows a consistent, almost linear, behavior with respect to the temperature of an isothermal source. This special behavior serves as a smoothing factor while solving for the unknown strength. Thus, a very good and accurate estimation of Gr is achieved. The same reasoning can be applied to isoflux results.

The tendency to linear behavior for the temperature with respect to Gr grows stronger as the sensor locations move towards the trailing edge of the plate. Based on this observation it was predicted that optimum sensor location would be close to the trailing edge. For the isothermal problem, PSO proved this prediction with the outcome location of 0.98L.

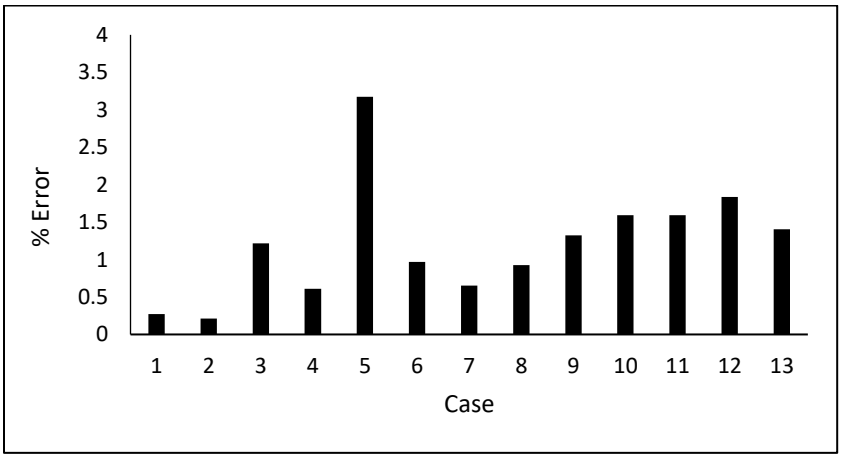

Figure 4-4- Source strength estimation error for isothermal boundary condition

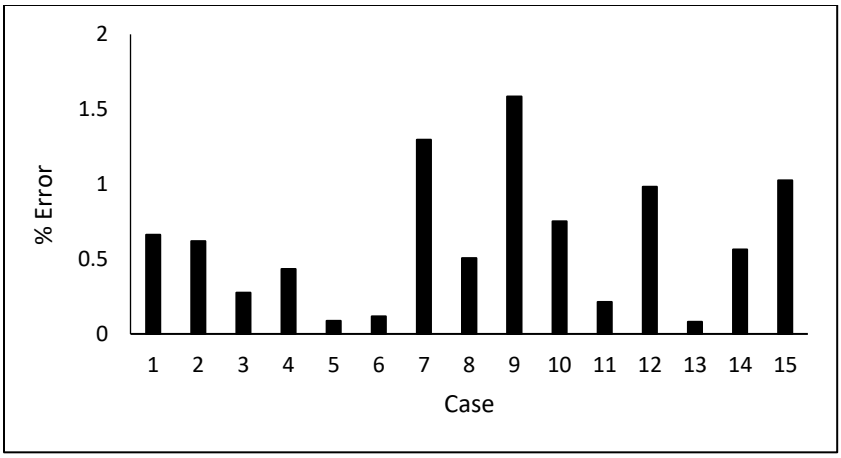

Figure 4-5- Source strength estimation error for isoflux boundary condition

4.2.2 Type II: Unknown source location

Here, it was assumed that source strength is known. Again, given that there is only one unknown, PSO was used to find the best single sensor location. Each particle is a location on the upper half of the plate. Equation (4-7) is the simplified objective function for this problem.

$$ObjectiveFunction = \sum_{i=1}^{N} \left| \frac{l_{est-i} - l_i}{l_i} \right| \Big/ N \tag{4-7}$$

The best sensor locations are given in Table 4-4 for isothermal and isoflux source types. Figure 4-6 and 4-7 show the estimation error results for isothermal and isoflux testing data sets respectively. Location estimation is more challenging due to the more complex relationship between temperature and source location, as a result of the strong dependence of flow on location. Based on equation (4-5), the source location has a more dominant effect on locations closer to the source rather than locations closer to the trailing edge, as is seen in Figure 4-3 and Table 4-1. Based on this observation, it was predicted that a

location closer to the mid-plane, which was the lower bound constraint for the particle selection, would better estimate the location. PSO again justified this prediction by giving a sensor location of 0.54L as the best suitable one.

The distance between the sensor and the source and its effect on estimation accuracy in isothermal cases is quite intriguing. While cross-referencing the highest percentage errors in Figure 4-6 with data from Table 4-2, it was concluded that the cases with highest estimation errors are the ones that have the largest distance between the source and the sensor location, indicating a relation between the accuracy of estimation and the distance of the source to sensor. This was expected based on observations made from Figure 4-3-b. The source location has a stronger effect on temperature trends when the sensor location is in close proximity. As distance increases, source location effect fades away and source strength becomes the dominant factor. It could be concluded that the method presented here would struggle with location estimation when the sensor is relatively far from the isothermal source. Cases 9 and 12 in Figure 4-6 reinforce this claim.

The same can be said about the isoflux cases except that the source location effect, based on Figure 4-3-d, is stronger and does not fade away as fast as in isothermal cases. This means that the optimum sensor location does not need to be very close to the lower bound of the search domain. PSO found a sensor location at 0.88L to be the optimum.

There are also other factors affecting the accuracy of the results. Inverse problems, as was mentioned earlier, are mathematically ill-posed problems and so they would inevitably introduce some challenges that are not physically justifiable. Location estimation error for case 1 in Figure 4-7, is an example of such challenges. This case has the same distance to

the sensor as case 5. However, case 5 has the highest and case 1 has one of the least estimation errors. Here, case 1 is not following the trend of other similar cases.

Table 4-4- Optimization Results for Single Unknown Problems

Problem		Best Location	Objective Function
Isothermal	Gr unknown	0.98L	0.0071
	Location unknown	0.54L	0.0375
Isoflux	Gr unknown	0.99L	0.0061
	Location unknown	0.88L	0.0278

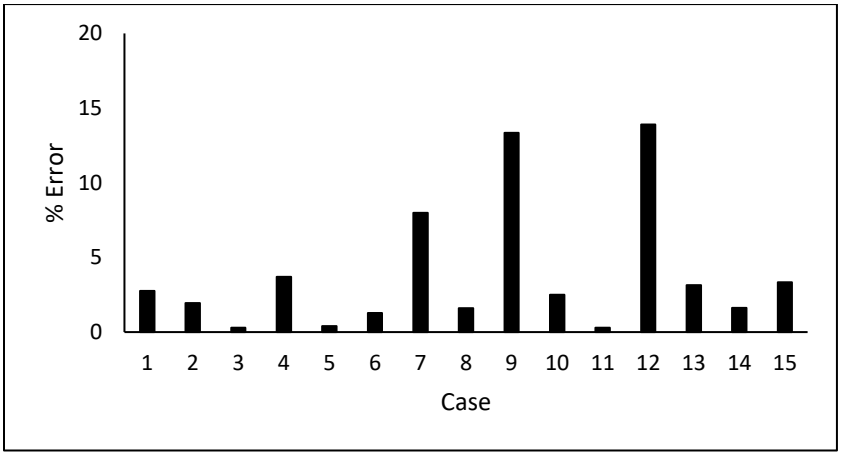

Figure 4-6- Source location estimation error for isothermal boundary condition

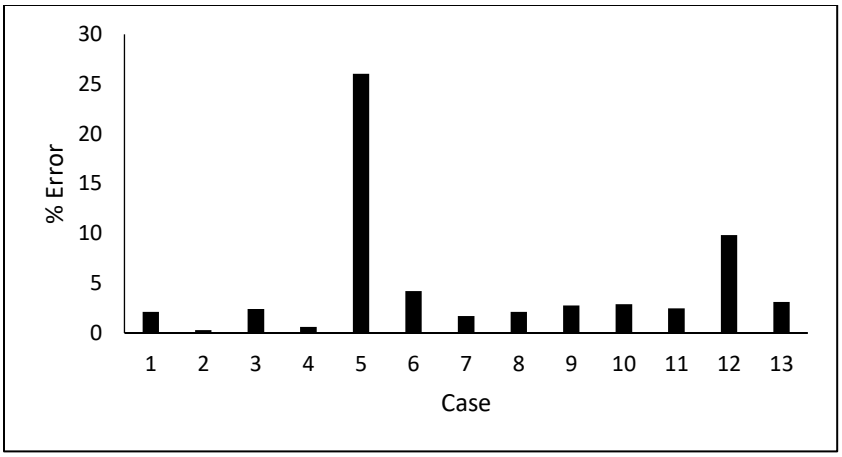

Figure 4-7- Source location estimation error for isoflux boundary condition

4.2.3 Type III: Unknown source strength and location

In this part, both source inputs, strength, and location were assumed to be unknown. As discussed earlier, a pair of locations are needed to estimate these unknowns. In this part, each particle represents a pair of locations. Table 4-5 summarizes the optimization results for both isothermal and isoflux scenarios. Figure 4-8 and 4-11 show the estimation errors for Gr and l when using the locations given by PSO for isothermal and isoflux scenarios respectively. Source strength and locations for all cases are summarized in Table 4-2 and 4-3 for isothermal and isoflux scenarios respectively.

Table 4-5- Optimization Results for Two Unknown Problem

	Best Pair	Corresponding Location	Objective Function
Isothermal	15 , 60	0.61L , 0.98L	0.0269
Isoflux	25 , 57	0.69L , 0.95L	0.0268

Based on previous observations, it was expected that a suitable pair of locations would be close to the trailing edge, to better capture the effects of Gr, and close to mid-plate locations, to better capture the effects of location change. Results from PSO for isothermal source agreed with this expectation. Location 0.98L was already chosen to be the best suitable location for unknown source strength. This location showing up in the results could be a sign that equation (4-5) is at its best when capturing the temperature trend with respect to Gr. Similar to the location unknown problem, cases with highest location estimation error have the largest distance for the sensor locations, proving that putting a sensor as close as possible to the vicinity of the unknown sources is the key to have a good and reliable estimation. Earlier results from the location unknown problem confirm this claim. Of course, in practice, just like this study, there are various constraints on the location of sensors. The same could be said for the isoflux source type problem. Given that the source location effect in the isoflux source is stronger, sensors could be placed further away compared to the isothermal scenario and still produce results with reasonable accuracy.

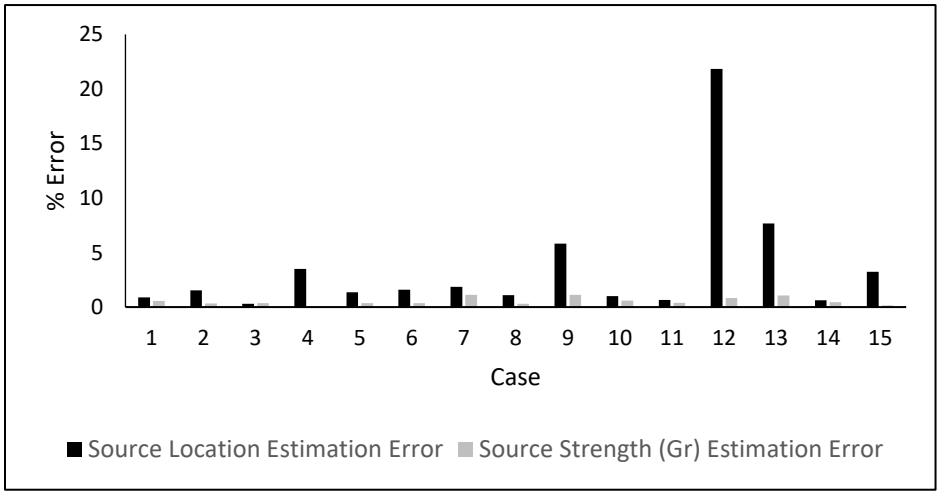

Figure 4-8- Source strength and location estimation error for isothermal boundary condition

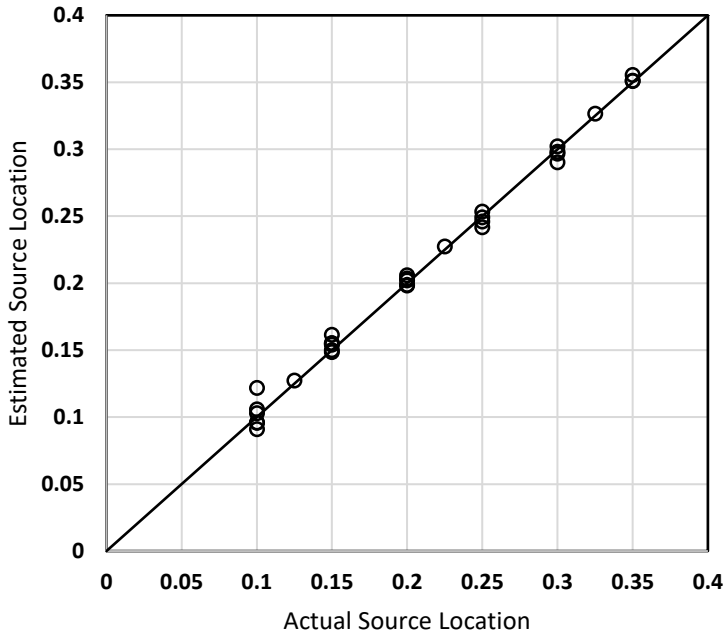

Figure 4-9- Actual vs estimated source location using two sensors - Isothermal

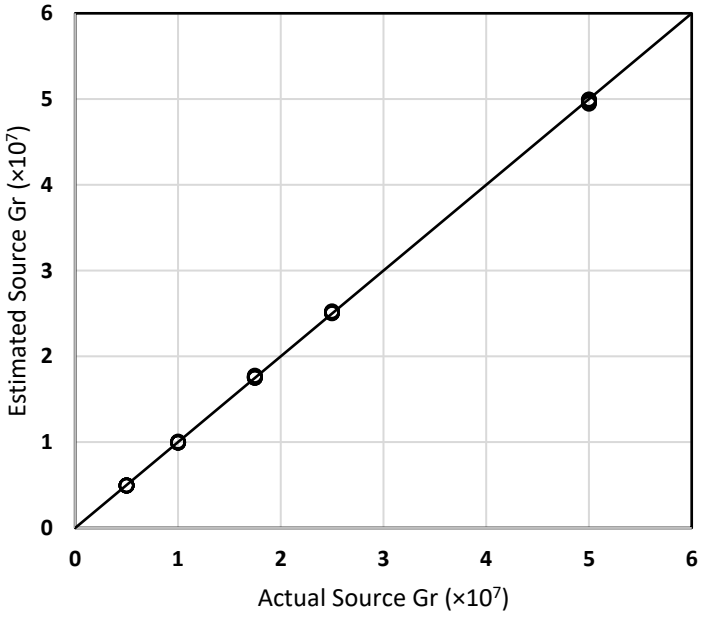

Figure 4-10- Actual vs estimated source strength using two sensors – Isothermal

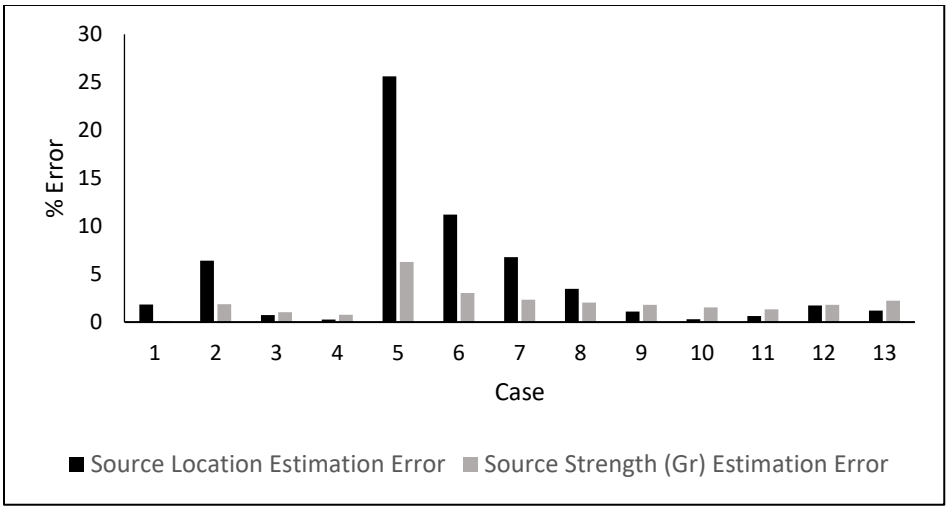

Figure 4-11- Source strength and location estimation error for isoflux boundary condition

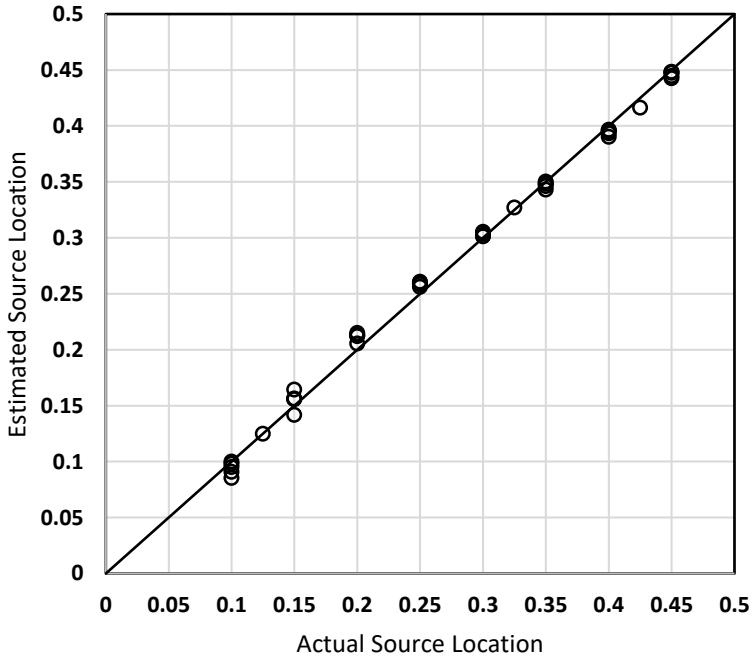

Figure 4-12- Actual vs estimated source location using two sensors - Isoflux

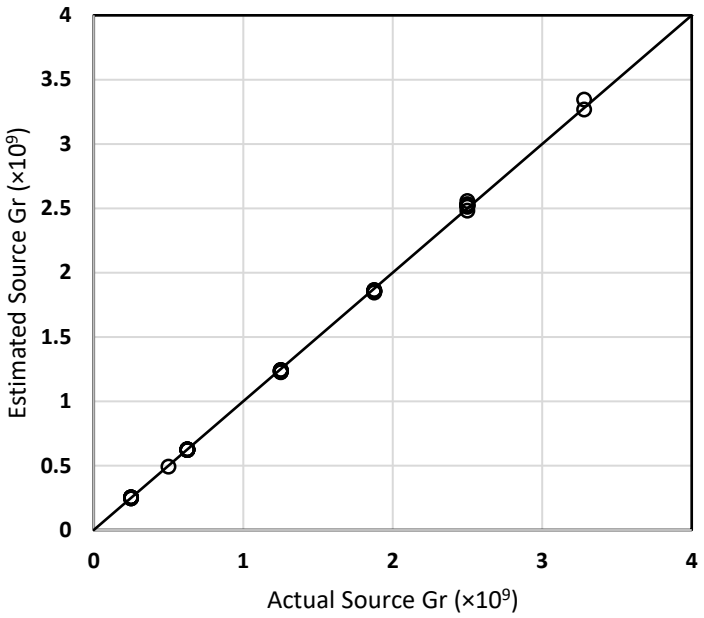

Figure 4-13- Actual vs estimated source strength using two sensors – Isoflux

Figure 4-9 and Figure 4-12 show the actual versus estimated source location for the entire data set of isothermal and isoflux boundary conditions, respectively. These plots confirm the claim that sources that are further away from the sensors have the highest location estimation error. Figure 4-10 and Figure 4-13 represent the actual versus estimated source strength for isothermal and isoflux scenarios. It should be noted that these plots also contain both training and testing data sets results. It is clear from these plots that the algorithm is capable of estimating source strength with a high level of accuracy.

4.3. Conclusion

In this chapter laminar wall plume forward problem was studied. These wall plumes were caused by both isothermal and isoflux boundary conditions. An observation was made on how the steady-state temperature on the wall behaves relative to plume heat input and

location. Various functions were studied to capture this behavior and equation (4-5) was selected. Using this interpolating function, the inverse methodology developed in chapter 3 was tested on the forward problem data. PSO provided optimum locations to put sensors to read the steady-state temperature on the wall. Using these sensors three different types of inverse problems were solved.

It was shown that temperature trends on the wall get closer to linear change with respect to plume strength further downstream of the source. As a result, putting a sensor near the trailing edge of the wall could help with an accurate estimation of heat input when dealing with unknown source strength problems. On the other hand, location estimation depends on sensors that are closer to source location as the effects of source location are more intense when the source is closer to the sensor. A well-placed sensor near the middle of the plate would accurately estimate unknown source locations. Finally, a combination of the two was found to produce the best inverse results for problems in which both source strength and location were unknown.

Chapter 5: Inverse solution – Using Transient Data

In this chapter, transient temperature data is used to solve the inverse heat convection problem of a wall plume. A detailed study of the transient flow behavior is discussed in the following section.

5.1. Physics of the Forward Problem

Transient flow results and data of the wall plume problem discussed in chapter 4 are studied for several different cases. For a short time at the beginning of the flow, the temperature behavior of the fluid next to the heated segment of the wall follows the classic conduction-only solution suggested by the literature. However, as expected, it soon changes to a two-dimensional transient convective flow and eventually reaches the steady-state.

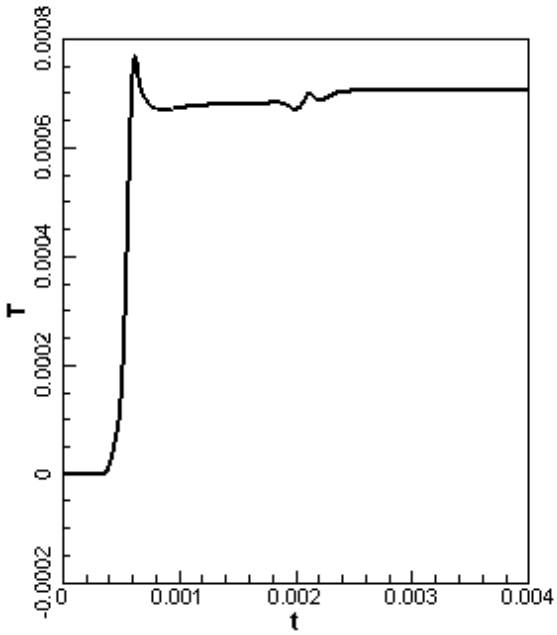

Figure 5-1- Non-dimensional temperature history at x=0.4 on the wall (Gr = 2.5×10^{10} and l = 0.2).

Figure 5-1 shows the temperature history at a given location downstream of the source on the wall. The leading-edge effect can be seen to reach the downstream location with a delay. It is worth noting the temperature seems to have an overshoot, or a local maximum, before dropping and eventually reaching the steady-state. That overshoot is caused by the movement of the initially heated bulk of the fluid. This bulk of fluid gets heated up in the conduction-only phase without moving, so when it finally starts to move downstream, it brings a considerable amount of energy with it and, as a result, a temperature overshoot is observed. The fluid that follows this bulk, does not have the same amount of stored energy as it does not go through the stationary conduction-only heating phase.

Figure 5-2 shows that the local maximum dwindles as the flow goes further downstream. A possible explanation is that the heated bulk of fluid expands and dissipates into a vortex in the y-direction, normal to the wall, as it flows downstream. Considering that it carries a set amount of energy, the quantity of energy per unit area decreases and thus the local temperature on the wall dwindles as a result. Figure 5-3 illustrates the expansion of the bulk as it goes downstream. It shows the y-direction expansion of the bulk vorticity. The fluid has to rotate back towards the plume outside of the boundary layer to satisfy continuity. In this recirculation, the bulk fluid gains a velocity component in y-direction that, in time, expands the flow in the y-direction. If a horizontal line is drawn at any location downstream of the plume, like in Figure 5-3, the effects of the flow first reach the line at a position away from the wall. As the flow goes downstream and expands in the y-direction, this position moves further away from the wall. This initial vortex expansion continues to a point downstream of the flow that the initial peak temperature on the wall is less than the final steady-state value.

Another interesting observation is that at locations further downstream, temperature changes in a more complex way in comparison with the locations closer to the plume source. Figure 5-2 shows that at x = 0.4, the temperature reaches steady-state value after the initial peak has passed without many fluctuations, but at x = 0.8, temperature undergoes two local minima and then rises to its steady-state value. The reason for this behavior is in the first column of Figure 5-2 where it can be seen that the flow vortex is accelerating faster than it is expanding. In other words, the initial bulk of fluid accelerates and passes through the locations closer to the plume source before the vortex has the opportunity to expand and some of the bulk fluid start to rotate downwards towards the upstream. Therefore, locations upstream, that are closer to the plume source, reach the steady-state condition faster than those that experience the vortex rotational flow.

Figure 5-3 also shows a trend in transient behavior across the temperature boundary layer. After reaching a maximum, the temperature peak breaks into two local maxima, one of which moves towards the wall over time and reaches a peak value at steady-state while the other moves away from the wall and dwindles in magnitude until the temperature reaches the value of the ambient fluid. The fluid that accelerates downstream after the initial bulk has moved is not expanding in the y-direction, normal to the wall, so there is no more heated fluid to fill the space left by the initial bulk moving fluid and the ambient fluid fills the gap. This explains the schism in temperature across the transient boundary layer and the decrease of the local maximum away from the wall.

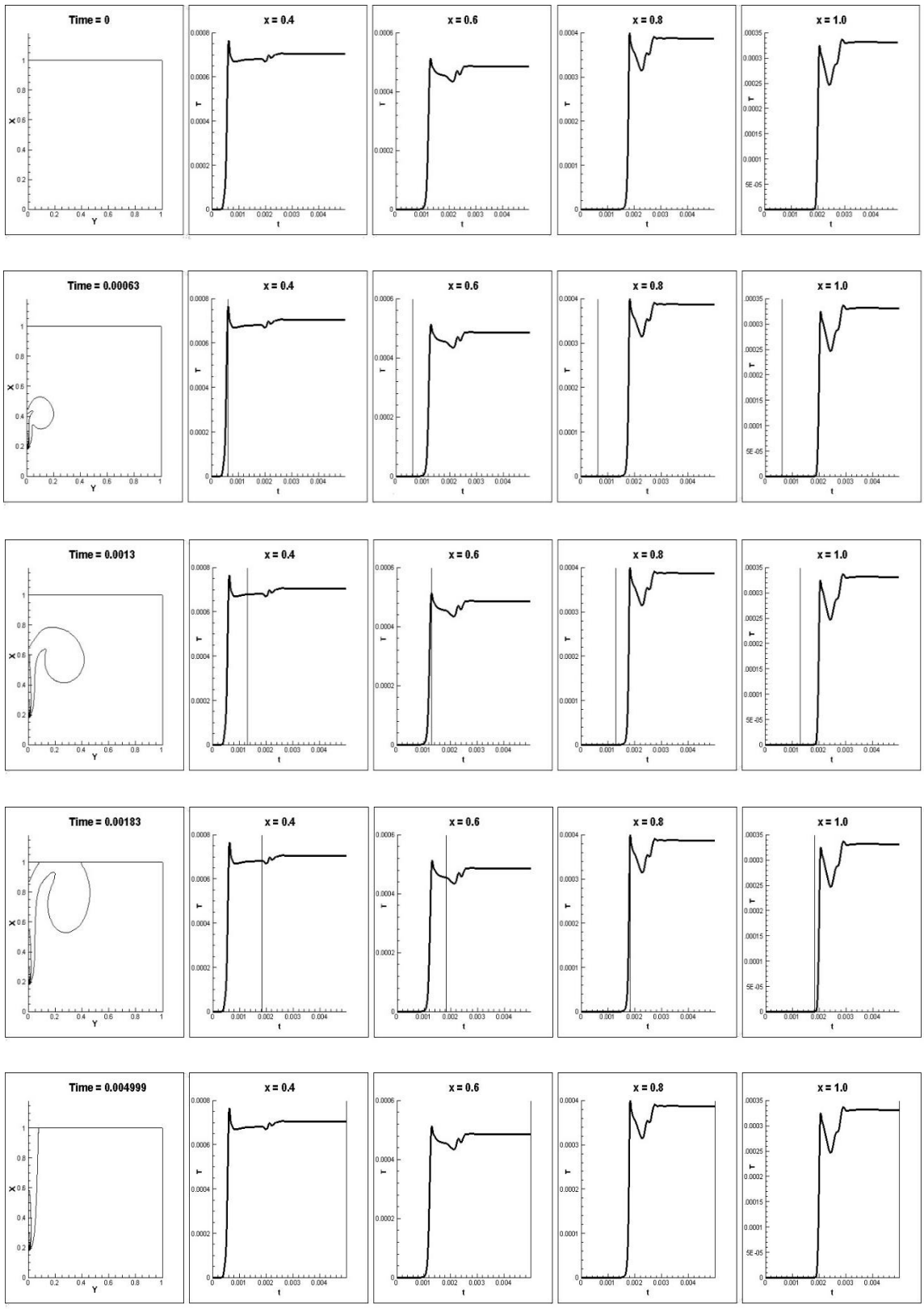

Figure 5-2- Transient temperature development (Gr = 2.5×10^{10} and l = 0.2).

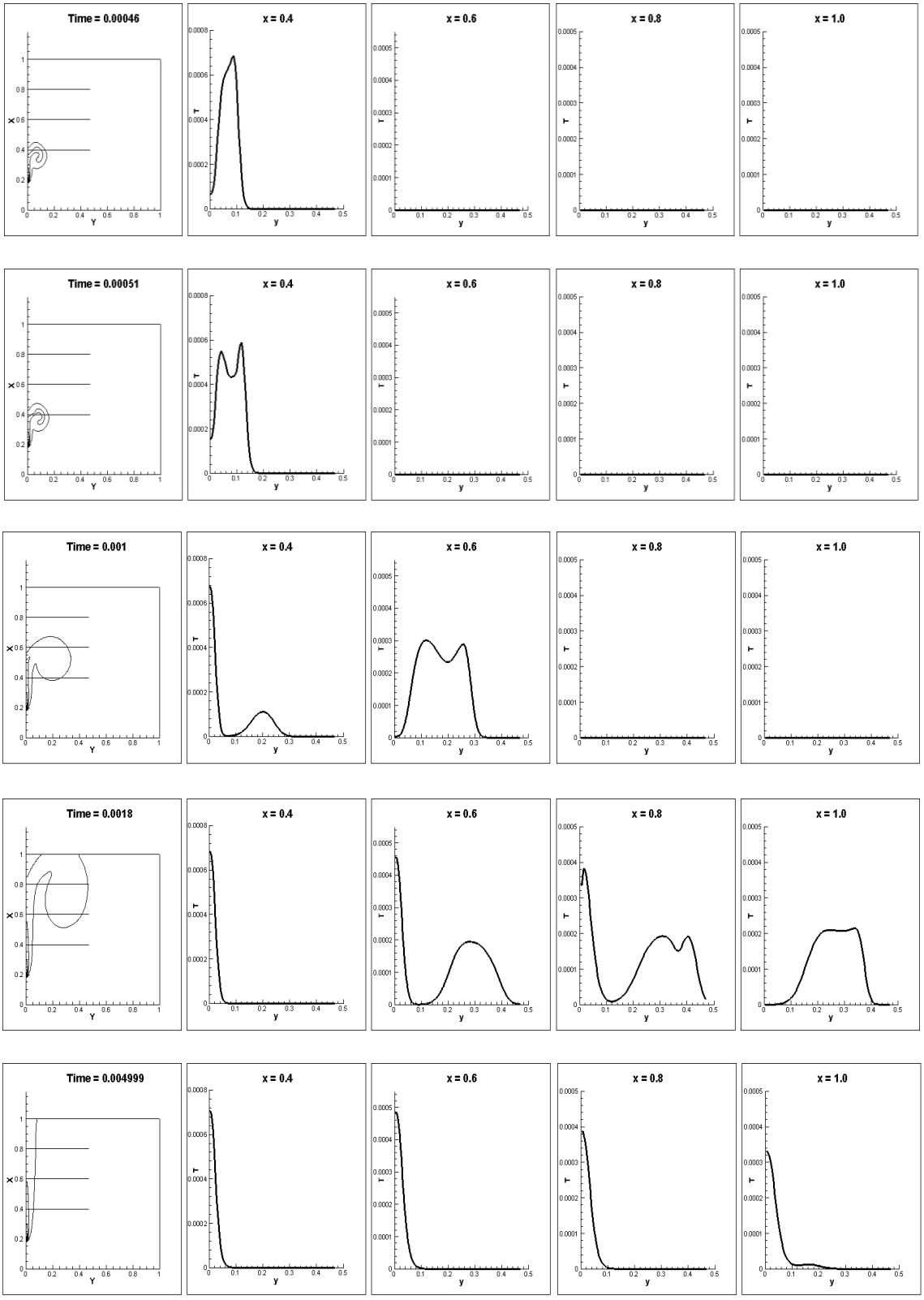

Figure 5-3- Temperature envelope development (Gr = 2.5×10^{10} and l = 0.2).

Time for initial temperature rise, time at which peak temperature occurs and peak temperature value are some of the interesting observations of Figure 5-2. If by using regression methods, relevant interpolative equations are achieved that relate any of the these discussed observations to plume source and its location, then they could be used to solve the inverse problem. The idea here is to relate the flow features at each location downstream of the flow to the plume source strength and location. With such relations at hand, one can pick at least two locations on the wall and solve the resulting system of equations to solve for the plume strength and location.

The variation of Peak Temperature Time (PTT) with source strength has been plotted in Figure 5-4 at different locations on the wall for the same source location. It is also seen that at each location, the following equation can be used to relate the PTT to the plume Gr number:

$$PTT(Gr) = \frac{a_1}{Gr^{a_2}} \tag{5-1}$$

where Gr is Grashof number and a_1 and a_2 are coefficients calculated at a location on the wall using regression methods. A group of 10 cases was used to obtain the coefficients. Table 5-1 shows the coefficients for the four locations on the wall, shown in Figure 5-4, along with their correlation coefficients. PTT estimated by equation (5-1) is also plotted in Figure 5-4 for each location. The decreasing trend of the plot is expected. As the plume strength increases, the fluid adjacent to the heating area absorbs more energy and accelerates more rapidly and reaches a downstream location faster. As a result, the difference in PTT for different locations on the wall for the same plume strength decreases as the plume gets stronger.

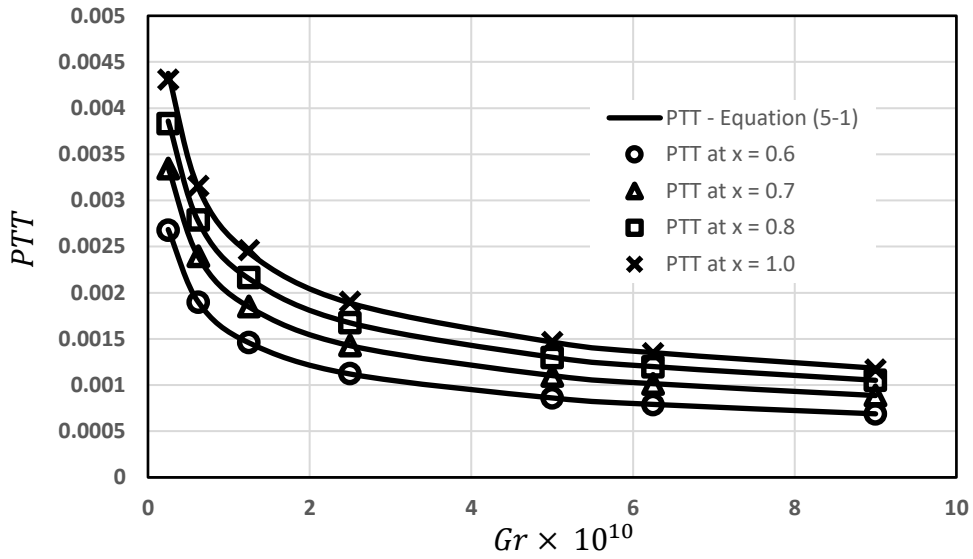

Figure 5-4- Peak Temperature Time (PTT) variation with respect to plume strength at different locations on the wall (l = 0.25).

Table 5-1- Equation (5-1) coefficients for different heights on the wall (l = 0.25).

Height	a_1	a_2	R^2
0.6	9.96	0.379	0.999
0.7	10.383	0.371	0.999
0.8	9.91	0.363	0.999
1.0	11.80	0.365	0.999

PTT variations with respect to source location are presented in Figure 5-5. For a wall plume on a semi-infinite plate due to a line source, source location would linearly affect the temperature and velocity profiles in the downstream areas. For the corner flow of the problem, it was expected that the plume location effects on temperature deviate from linear form, based on the distance between the plume and the corner. The boundary layer on the bottom would interfere with the boundary layer development of the plumes very close to the corner on the wall and hence leaves an effect on the resulting temperature profiles downstream of the plume. Figure 5-5 shows that, if the source location is reasonably far

away from the corner, the deviation is negligible, and a linear variation is observed. At each height, the following equation can be used to relate the PTT to the plume location:

$$PTT(l) = b_1 l + b_2 \tag{5-2}$$

where l is plume location and b_1 and b_2 are coefficients calculated at any height on the wall using regression methods. Table 5-2 shows the coefficients for the four heights on the wall, shown in Figure 5-5, along with their correlation coefficients.

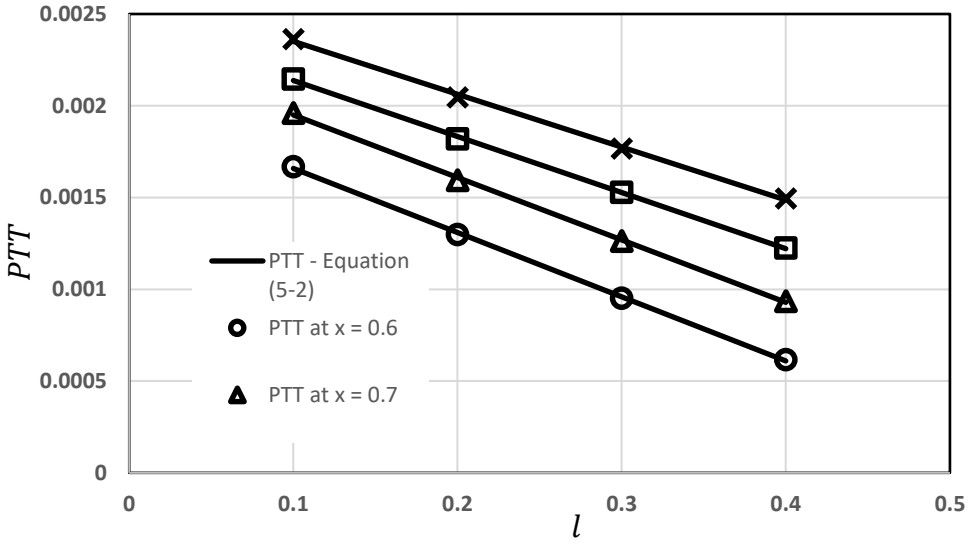

Figure 5-5- Peak Temperature Time (PTT) variation with respect to plume location at different heights on the wall (Gr = 2.5× 10^{10}).

Table 5-2- Equation (5-2) coefficients for different heights on the wall (Gr = 2.5× 10^{10}).

Height	b_1	b_2	R^2
0.6	-0.003496	0.00201	0.999
0.7	-0.003403	0.00229	0.999
0.8	-0.003054	0.00244	0.999
1.0	-0.002881	0.00264	0.998

The next step is to try and find a function that can predict PTT based on both source strength and location. The function presented in this article is a combination of equations (5-1) and (5-2) in the form of equation (5-3):

$$PTT(Gr, l) = \frac{c_1 l + c_2}{Gr^{c_3}} \tag{5-3}$$

Equation (5-3) captures the PTT behavior with respect to both source strength and location. Clearly, this is not unique and other representations can similarly be considered. Coefficients c_1, c_2 and c_3 are found using nonlinear, multivariable regression methods. Table 5-3 summarizes some of the equation (5-3) coefficients along with their correlation coefficient or R^2 values. A closer look at the coefficients shows that if the data of Table 5-1 and 5-2 are combined they result in numbers very close to the ones provided in Table 5-3, supporting the idea that PTT behavior can be modeled with a separation of the variable approach described by equations (5-1) and (5-2).

Equation (5-3) is unique for any given height on the wall and can predict the PTT. If at least two sensors are located downstream of the plume, a system of the equations, with unique coefficients for their respective sensor locations, can be solved to find Gr and l. Two is the minimum number of sensors that this method can work with since we want both the strength and location of the source. By adding more sensors, additional equations are obtained and as a result, the problem shifts from solving a nonlinear system of equations to nonlinear curve fitting. For nonlinear curve fitting, Levenberg-Marquardt [66] algorithm is used. A more detailed discussion on the effects of the number of sensors on the performance of the method is provided later in the text.

Table 5-3- Equation (5-3) coefficients for different heights on the wall.

Height	c_1	c_2	c_3	R^2
0.6	-29.8215	17.2668	0.378	0.997
0.7	-25.5308	17.37276	0.373	0.997
0.8	-19.7253	15.78299	0.366	0.999
1.0	-17.6432	15.95638	0.363	0.999

Regardless of the number of sensors, it is important to choose the best sensors to solve, or curve fit, the system of equations. PSO algorithm is used again to find the sensor locations that yield the least estimation errors. The training data set is used to find the coefficients of equation (5-3) and with the PSO algorithm to find the best sensor locations. These sensors are then tested by a new set of cases, called testing data set, to check the validity and robustness of the method.

5.2. Results

In this section, the results for three different types of problems are presented. Type I where the source strength is unknown, type II where the source location is unknown and finally type III where both source location and strength are unknown. For each problem, equation (5-3 coefficients and optimal sensor locations are found using the training data set. For each category, the objective function of equation (3-5) is modified to better suit the specific problem. Due to the stochastic nature of PSO, the algorithm is repeated a number of times with random particles each time to populate the initial swarm. The following results are the most frequent ones with the least objective function values.

5.2.1 Type I: Unknown source strength

There are many scenarios where the location of the plume is known, for example, the location of an electronic chip on the wall is known but when it overheats the amount of heat input is unknown. For such cases, because only one parameter is unknown, in theory, a single sensor is enough to solve the inverse problem. Equation (5-3) and the modified objective function of equation (4-6) were used together with the PSO algorithm to locate the best point to put the sensor.

Figure 5-6 shows the actual vs estimated source strength. The presented method has performed well in estimating the plume strength. With just a single sensor, this method achieved an average estimation error of 2.71% with a maximum error value of 14.02%. In order to study the effects of increasing the number of sensors on the accuracy of the method, two and three sensor scenarios were studied as well. Increasing the number of sensors influences both the maximum error value and the standard deviation of the error. Error average and standard deviation values along with the location of the optimum sensors are gathered in Table 5-4 for one, two and three sensors problems. Increasing the number of sensors from one to two and three decreases the maximum error value from 14.02% to 9.02% and 8.52%, respectively, while decreasing the standard deviation from 2.7% to 2.14% and 2.09%. While adding more sensors does not change the average error percentage dramatically, it reduces the maximum error value to an acceptable range and also dampens the standard deviation value. Therefore, when using three sensors, for instance, while the average error is the same as the case of one sensor, there is a higher chance that all the estimations even those that are above the average, are in an acceptable error range.

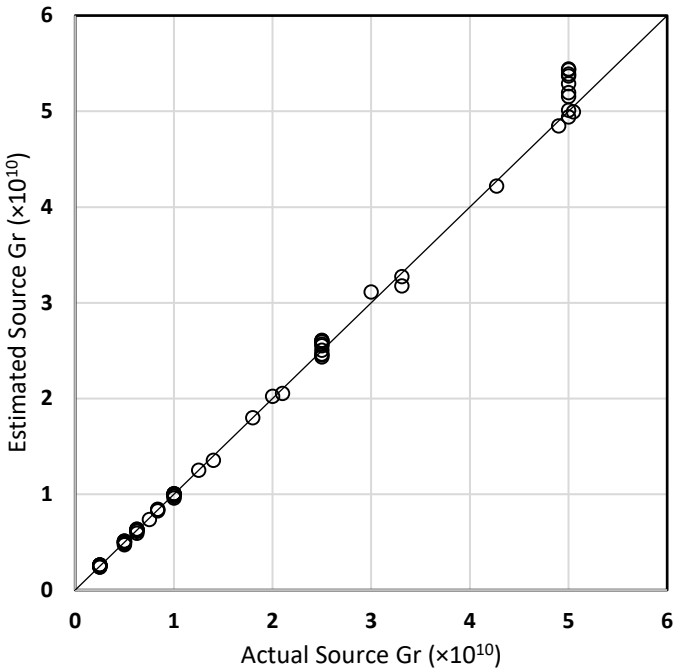

Figure 5-6- Actual vs estimated source strength using one sensor

Table 5-4- Optimum sensor data – plume strength unknown.

Number of sensors	Location on the wall	Average % Error	Standard Deviation
1	0.99L	2.71	2.70
2	0.78L, 0.98L	2.12	2.14
3	0.76L, 0.8L, 98L	2.11	2.09

5.2.2 Type II: Unknown source location

There are scenarios in which the strength of the plume is known but the location is unknown. As discussed earlier, because only one parameter is unknown, a single sensor should be enough to solve the inverse problem. Equation (4-7), the modified objective function, is used along with equation (5-3) in the PSO algorithm.

A graph of actual versus estimated source location is shown in Figure 5-7. Overall the accuracy of the method is acceptable with an error average of 1.90% but the maximum error value of 7.42% leaves room for improving the setup. Increasing the number of sensors is the next logical step. The problem was solved with the condition that two and three sensors were available. By increasing the number of sensors, the maximum error value is increased from 7.42% in single sensor case to 7.55% and 9.83% in two and three sensor cases. Table 5-5 shows the optimum sensor data for type II problems. Based on this data, while the maximum error value has increased, the average estimation error and standard deviation values have slightly increased as well. A possible explanation is that due to the linearity of the plume location on PTT shown in equation (5-3), increasing the number of input data introduces more regression related uncertainty rather than improving the overall accuracy of the results. It is worth mentioning that although increasing the number of sensors seems to be lowering the accuracy, estimation errors are still in an acceptable range.

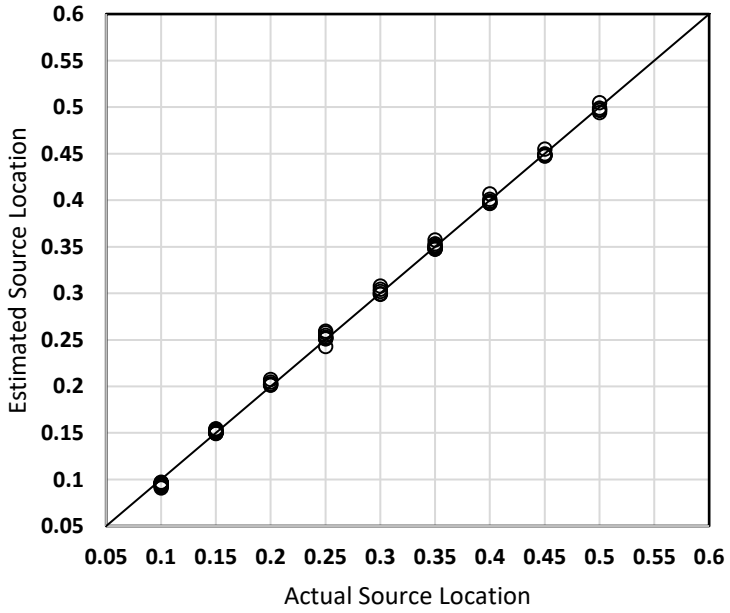

Figure 5-7- Actual vs estimated source location using one sensor

Table 5-5- Optimum sensor data – plume location unknown.

Number of sensors	Best Points	Location on the wall	Average % Error	Standard Deviation
1	17	0.63L	1.90	1.89
2	14, 19	0.61L, 65L	1.92	1.97
3	5, 13, 20	0.53L, 0.59L, 0.66L	2.19	2.39

5.2.3 Type III: Unknown source strength and location

Finally, the last problem involves both plume location and strength as unknowns. This is of practical interest in environmental problems when the source strength and location are both important. The Algorithm is first tried with the assumption that only two sensors are needed. Each initial particle then consists of a vector of two randomly chosen points. Based on type I and II problems discussed earlier it is expected that by increasing the number of sensors or data points, the accuracy of the method will improve, therefore two more scenarios were studied. Figure 5-8 and 5-9 show a comparison between the estimation results of source strength and location, respectively, while using 2 and 4 sensors. It is clearly shown that by adding more sensors the accuracy of the method improved drastically. In the case of only 2 sensors, although the majority of estimation errors, for both plume strength and location, are in a good range, there are cases with very high errors, especially when estimating the location.

The maximum plume location estimation error percentage has decreased from 392.61% with two sensors to 4.06% with three, and 3.89% with four sensors. The same trend is seen with the plume strength estimation where the maximum error percentage reduces from 300% with two sensors to 10.31% and 10.38% with three and four sensors respectively. Increasing the number of sensors improves the estimation errors drastically. This

improvement ensures that overall this method would provide results within an acceptable error range. Table 5-6 provides average and standard deviation values for each scenario as well as the optimized sensor locations.

While the increase in a number of sensors does not improve the accuracy in type II problems, it greatly increased the accuracy in location estimation in type III problems. It can be concluded that in application, putting at least three sensors on the wall, could provide satisfactory results for all three types of problems. The reason that three is chosen over four sensors is that, although four sensors provide better results, the difference does not justify the overall added complexity and cost to the system, as it can be seen by the data gathered in Table 5-6.

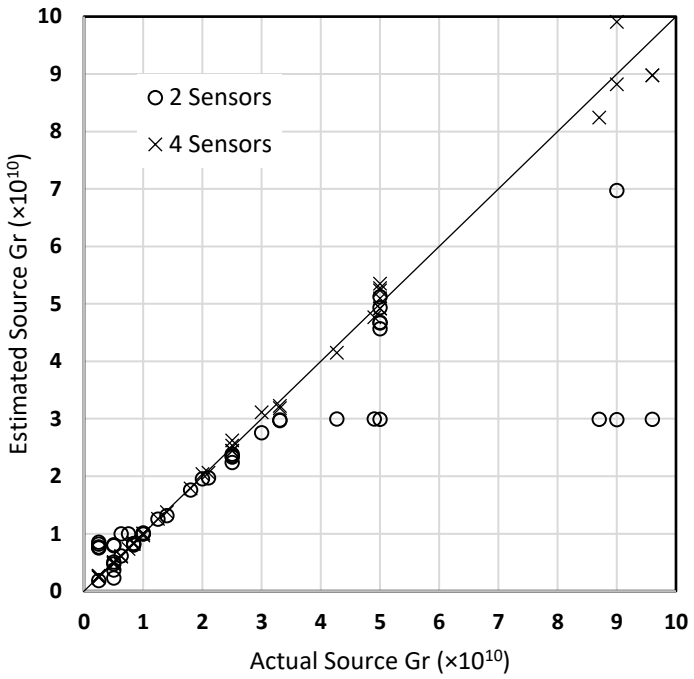

Figure 5-8- Actual vs estimated source strength - comparison between 2 and 4 Sensors

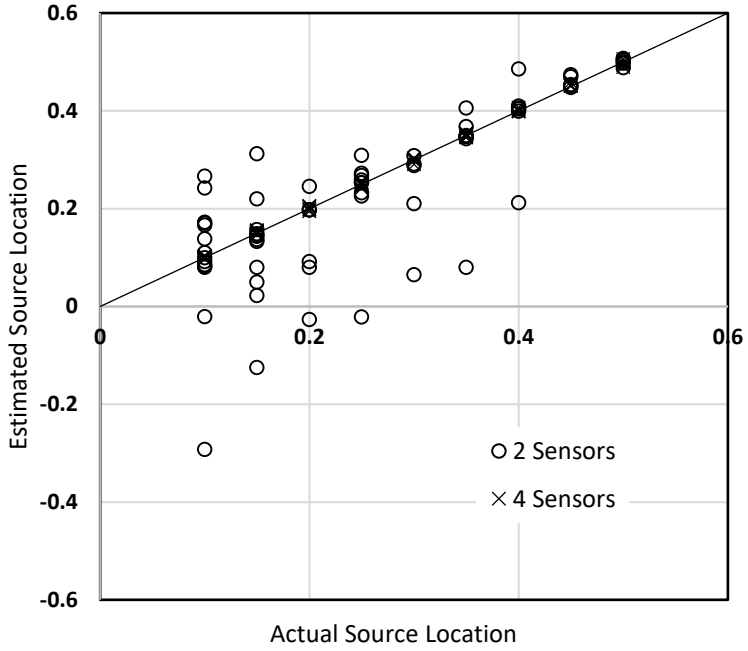

Figure 5-9- Actual vs estimated source location - comparison between 2 and 4 Sensors

Table 5-6- Optimum sensor data – plume strength and location unknown.

Number of sensors	Location on the wall	Average % Error - *l*	Standard Deviation - *l*	Average % Error - *Gr*	Standard Deviation - *Gr*
2	0.71L, 0.85L	35.32	62.50	41.00	68.28
3	0.59L, 0.78L, 0.92L	1.29	1.03	2.94	2.17
4	0.58L, 0.63L, 0.78L, 0.92L	1.23	0.95	2.89	2.16

It is worth discussing how the three optimum sensors for type III, which is the most general type, would estimate the unknowns in type I and II problems. Type I and II are solved using the three optimum sensors of type III. Table 5-7 and 5-8 summarize the results. As it is expected the overall results are not as good as the ones obtained with the optimum sensor locations, however, they are in a very acceptable range. From these data, it can be

concluded that three is the optimal number of required sensors to get good results all around. This conclusion was expected as two of these sensors at 0.59L and 0.78L are among the optimum sensors of type II and I respectively and contribute to acceptable results.

Table 5-7- Type I & II estimation errors using type III optimized three sensors from sample cases.

$Gr \times 10^{10}$		0.25	0.5	1	2.5	5
l						
0.1	Gr	2.89%	3.89%	2.99%	2.35%	2.50%
	l	6.59%	8.98%	6.98%	5.56%	5.87%
0.2	Gr	2.47%	0.15%	1.42%	3.75%	4.80%
	l	2.19%	0.26%	1.44%	3.46%	4.43%
0.3	Gr	2.48%	0.58%	1.02%	4.07%	7.58%
	l	1.04%	0.24%	0.60%	2.11%	3.79%
0.4	Gr	0.86%	0.29%	0.14%	2.09%	7.39%
	l	0.36%	0.10%	0.05%	0.71%	2.34%
0.5	Gr	5.39%	4.02%	1.98%	0.32%	4.52%
	l	1.47%	0.97%	0.44%	0.09%	1.09%

Table 5-8- Type I & II results using type III optimized three sensor

Type	Average % Error	Maximum % Error	Standard Deviation
I	2.30	8.23	2.21
II	2.46	11.53	2.61

5.3. Conclusion

In this chapter, transient wall plume flow due to a heat source located on the wall near a corner with a bottom wall was considered and basic transient features were observed and studied. Major interest points of this transient flow were temperature rise initiation time and peak temperature time. These times not only described the transient flow behavior and temperature dissipation downstream of the plume but also provided valuable insight to build an inverse solution. In the case of this article, peak temperature time or PTT was used in the search-based methodology to solve the inverse wall plume problem. The inverse method involves a series of interpolating functions relating peak temperature time to plume`s strength and location, and a search-based optimization algorithm. An interesting feature of this study was limiting the available data points. Only data points located on the wall were used in the search space to better model the practical applications where it is only applicable to put a sensor on the wall rather than an arbitrary location in the solution domain.

It was observed that for type I and II problems, where a single plume's feature, either its location or strength is unknown, the minimum number of sensors required by theory, i.e., one, is sufficient to achieve reasonably accurate results. An average estimation error of 2.71% for the case of unknown source strength and an average estimation error of 1.9% for the unknown location was obtained. The effects of the number of sensors were also studied and it was concluded that increasing the number of sensors slightly improves the case of unknown strength, from 2.71% to 2.11% average, but increases the average estimation error in the case of unknown location from 1.9% to 2.19%. Next, type III problems were studied. The minimum number of sensors required by the theory, 2, did not

produce reasonable results, with errors as high as nearly 400% in estimating the location of the plume. Increasing the number of sensors improved the results dramatically and the average errors reduced to 2.89% and 1.23% strength and location estimation, respectively. Based on the results provided, by improving the standard deviation value, increasing the number of sensors ensures that more solutions are in the acceptable error range. The performance of the three optimum sensors of the type III scenario was then tested for type I and II scenarios only to produce good results. It can be concluded that three sensors on the wall are enough to provide good results for any wall plume inverse situation.

Chapter 6: Inverse solution – Turbulent Steady-State Data

In this chapter, an inverse solution to the turbulent wall plume problem using relations between the steady-state temperatures on the plate and the location and strength of the plume is studied.

6.1. Physics of the Forward Problem

The geometry and boundary conditions of the corner wall plume flow were discussed in detail in chapter 4. Here, the heat input of the plume is high enough for the flow to land on the turbulent regime. Navier-Stokes equations need to be modified to capture the nature of the turbulent flow. For incompressible turbulent flow, velocity can be written as equation (6-1).

$$u_i = \overline{u_i} + \acute{u} \tag{6-1}$$

In this equation, $\overline{v_i}$ is the time-averaged value of the velocity (mean velocity) and $\acute{v}_\iota$ is the velocity fluctuation. Plugging equation (6-1) into the Navier-Stokes equation would result in an additional nonlinear term on the right-hand side, called the Reynolds stress, R_{ij}.

$$R_{ij} = -\rho\overline{\acute{u}_\iota \acute{u}_J} \tag{6-2}$$

The main challenge of modeling a turbulent flow is calculating the Reynolds stress. Boussinesq was the first to propose a closed-form solution by introducing the concept of kinematic eddy viscosity, υ_t.

$$-\overline{\acute{u}_i\acute{u}_j} = \upsilon_t\left(\frac{\partial\overline{u_i}}{\partial x_j}+\overline{\frac{\partial u_j}{\partial x_i}}\right)-\frac{2}{3}k\delta_{ij} \tag{6-3}$$

where k is the turbulent kinetic energy and δ is the Dirac delta function. The general idea here is to treat Reynolds stress like the viscous stress term by relating it to the fluid rate of strain. There are numerous models to calculate the eddy viscosity, such as Spalart-Allmaras, $k-\varepsilon$ and $k-\omega$ models. Each of these models introduces one or two more equations to the system of equations to find the unknown eddy viscosity. In this study, a standard $k-\omega$ turbulence method was used due to the fact that free convection flow regimes are usually in the lower Re ranges and $k-\omega$ generally works better with low Re turbulent flow regimes. $k-\omega$ introduces two transport equations to be solved along with the Navier-Stokes and energy equations: turbulent kinetic energy (k) and the specific rate of dissipation of kinetic energy (ω). Wilcox [67] $k-\omega$ model was used here.

$$\frac{\partial}{\partial x_i}(ku_i) = \frac{\partial}{\partial x_j}\left[\left(\upsilon+\frac{\upsilon_t}{\sigma_k}\right)\frac{\partial k}{\partial x_j}\right]+\upsilon_t\left[\left(\frac{\partial u_i}{\partial x_j}+\frac{\partial u_j}{\partial x_i}\right)-\frac{2}{3}k\delta_{ij}\right]\frac{\partial u_j}{\partial x_i}-Y_k \tag{6-4}$$

$$\frac{\partial}{\partial x_i}(\omega u_i) = \frac{\partial}{\partial x_j}\left[\left(\upsilon+\frac{\upsilon_t}{\sigma_\omega}\right)\frac{\partial \omega}{\partial x_j}\right]+\alpha\frac{\omega}{k}\upsilon_t\left[\left(\frac{\partial u_i}{\partial x_j}+\frac{\partial u_j}{\partial x_i}\right)-\frac{2}{3}k\delta_{ij}\right]\frac{\partial u_j}{\partial x_i}-Y_\omega \tag{6-5}$$

where σ_k and σ_ω are turbulent Prandtl numbers for k and ω, respectively. Also, Y_k and Y_ω represent the dissipation of k and ω. A few more equations are needed to close the above set of equations. The kinematic eddy (turbulent) viscosity, υ_t, is calculated using the following equations:

$$\upsilon_t = \alpha^*\frac{k}{\omega} \tag{6-6}$$

$$\alpha^* = \alpha^*_\infty\left(\frac{\alpha^*_0+Re_t/R_k}{1+Re_t/R_k}\right) \tag{6-7}$$

where $Re_t = \rho k/\mu\omega$, $R_k = 6$, $\alpha_0^* = \beta_i/3$ and $\beta_i = 0.072$. To calculate Y_k, equations (6-8) to (6-11) are used.

$$Y_k = \beta^* f_{\beta^*} k\omega \tag{6-8}$$

$$f_{\beta^*} = \begin{cases} 1 & x_k \leq 0 \\ \dfrac{1 + 680x_k^2}{1 + 400x_k^2} & x_k > 0 \end{cases} \tag{6-9}$$

$$x_k = \frac{1}{\omega^3}\frac{\partial k}{\partial x_j}\frac{\partial \omega}{\partial x_j} \tag{6-10}$$

For an incompressible fluid:

$$\beta^* = \beta_\infty^*\left(\frac{4/5 + (Re_t/R_\beta)^4}{1 + (Re_t/R_\beta)^4}\right) \tag{6-11}$$

To calculate Y_ω, equations (6-12) to (6-16) are used.

$$Y_\omega = \beta f_\beta \omega^2 \tag{6-12}$$

$$f_{\beta^*} = \frac{1 + 70x_\omega}{1 + 80x_\omega} \tag{6-13}$$

$$x_\omega = \left|\frac{\Omega_{ij}\Omega_{jk}S_{ki}}{(\beta_\infty^*\omega)^3}\right| \tag{6-14}$$

$$\Omega_{ij} = {}^1\!/_2\left(\frac{\partial u_i}{\partial x_j} - \frac{\partial u_j}{\partial x_i}\right) \tag{6-15}$$

For an incompressible fluid:

$$\beta = \beta_i \tag{6-16}$$

Ansys Fluent was used to model the turbulent flow along with the $k-\omega$ model. Considerations were made when generating mesh near the wall based on Henkes and

Hoogendoorn [68] extensive study of various turbulent natural convection models. Table 6-1 summarizes the closure coefficients used in equations (6-4) to (6-16).

In order to verify the turbulence model used, free convection flow next to a vertical plate was tested against Cheesewright [37] experimental data. Figure 6-1 shows that overall the temperature profiles are in good agreement.

Table 6-1- Coefficients used in $k-\omega$ turbulent model

σ_k	σ_ω	α_∞^*	α_∞	α_0	β_∞^*	β_i	R_β	R_k	R_ω
2	2	1	0.52	$1/9$	0.09	0.072	8	6	2.95

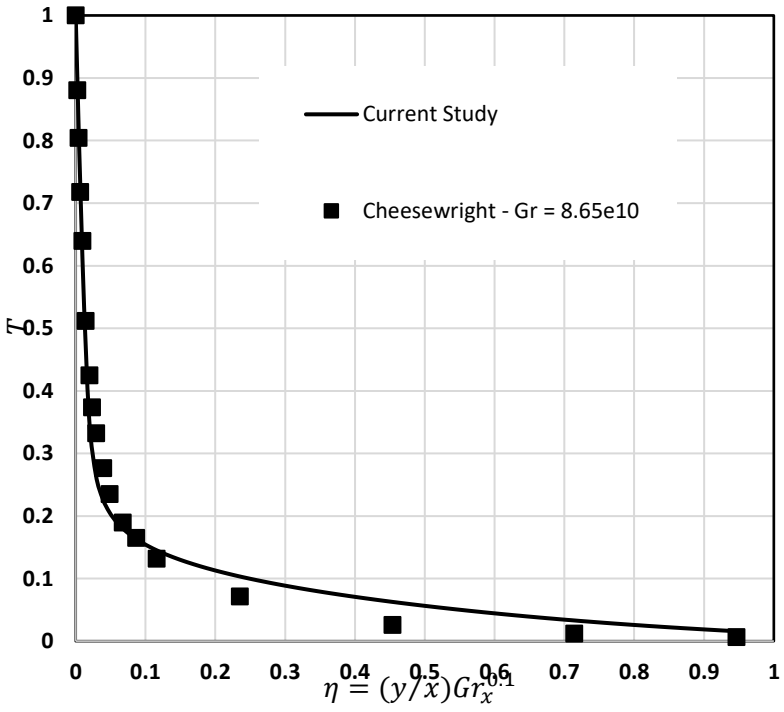

Figure 6-1- Turbulent boundary layer temperature comparison

For the laminar flow equation, (4-5) captured the relationship between the temperatures on the wall with plume location and heat input. By increasing the heat input and, as a result, the Gr number, plume flow characteristics would shift from laminar to turbulent. Here, in order to check the robustness of equation (4-5), it was assumed that the same equation could model the steady-state temperature readings on the wall. Only the coefficients were recalculated with the turbulent data. Similar to chapter 4, different combinations of source heat input and location were numerically simulated using the mentioned Fluent model. The temperature readings on the upper half of the wall were extracted from the simulation results. After determining the coefficients of equation (4-5) for all possible sensor locations using the extracted temperature readings, PSO would find the optimal locations to place sensors.

6.2. Results

Similar to the previous chapter, three different problems are presented: unknown source strength, unknown source location and finally unknown source strength and location. Equation (4-5) with turbulent coefficients was used with the inverse algorithm for each type of problem. The results are demonstrated here.

6.2.1 Type I: Unknown source strength

In this problem, it was assumed that source location is known. With this assumption, theoretically, only one equation is needed to estimate the strength. For type I problems, PSO uses the modified objective function, equation (4-6).

Figure 6-2 shows the actual versus estimated source strength. Inverse solution using equation (4-5) based on laminar temperature patterns performed well in estimating a

turbulent plume source heat input. Using a single sensor, this method produced results with an average error of 5.16% with a maximum error value of 13.69%. Based on Figure 6-2, the method has more difficulty estimating heat input when facing higher turbulent flows. The plot clearly shows the deviation from accurate estimation when the flow exceeds Gr = 75×10^{10}. This observation suggests that equation (4-5) can still predict temperature readings in the lower turbulent flows but needs some adjustments as the turbulence gets stronger. It should be noted, however, that the results are still in an acceptable range.

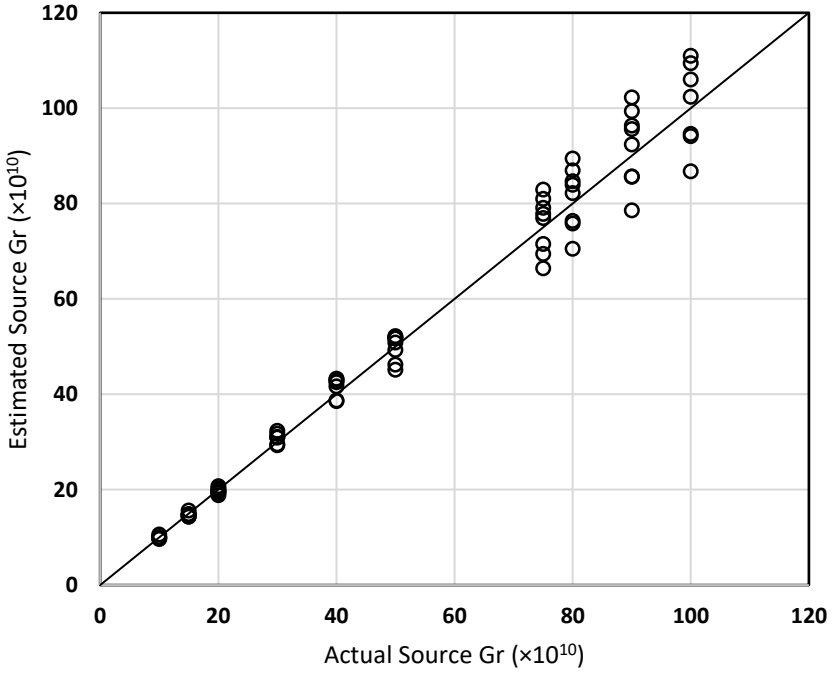

Figure 6-2- Actual vs estimated source strength using one sensor

Table 6-2- Optimum sensor data – plume strength unknown.

Number of sensors	Location on the wall	Average % Error	Standard Deviation
1	L	5.16	3.41
2	0.96L, L	5.16	3.42
3	0.91L, 0.96L, L	5.17	3.43

Two more scenarios with two and three sensors respectively were also considered to study the effects of additional sensors on the accuracy of the method. Table 6-2 summarizes the optimal sensor location as well as average, maximum and standard deviation for the error calculated in all the three scenarios. Based on the data, adding more sensors is not affecting the accuracy of the method.

6.2.2 Type II: Unknown source location

Type II deals with scenarios where the heat input of the source is known but the location is not. Like Type I, theoretically only one sensor is required to estimate the plume source location. PSO algorithm uses equation (4-7) as a modified version of the objective function.

Figure 6-3 shows the actual versus estimated source location. The inverse method provided solutions with an average error of 9.08%. The present method struggles the most with estimating sources that are close to the ground with a maximum error of about 57%. As was discussed in chapter 4, equation (4-5) is heavily influenced by source strength rather than location and as a result, it has difficulty estimating source locations that are relatively far away from the sensor. Figure 6-3 reinforces this observation. Estimations become more accurate as the source location gets closer to the sensor.

Scenarios with two and three sensors were also studied. Like type I problems before, adding more sensors is not affecting the accuracy of the method. Optimal sensor locations, average and maximum error values, and standard deviations are presented in Table 6-3.

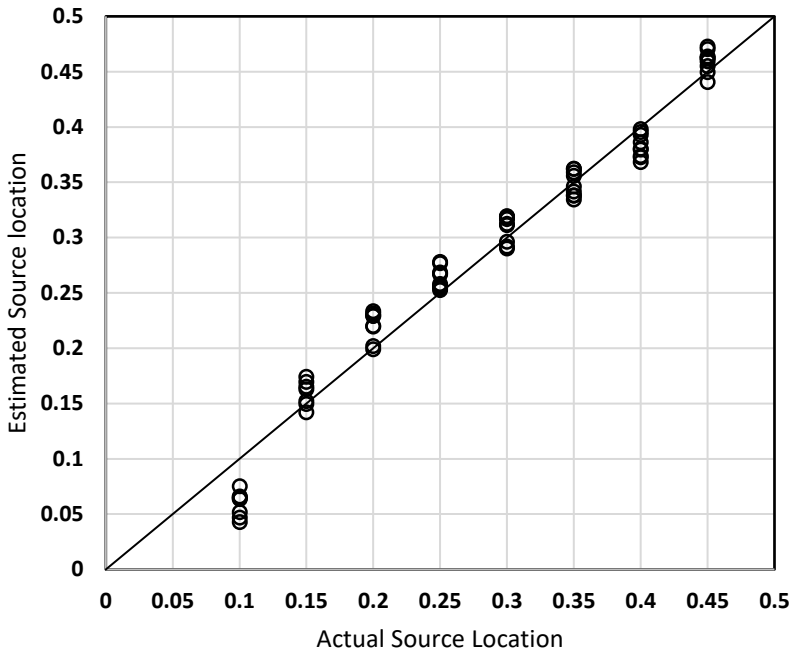

Figure 6-3- Actual vs estimated source location using one sensor

Table 6-3- Optimum sensor data – plume location unknown.

Number of sensors	Location on the wall	Average % Error	Standard Deviation
1	0.75L	9.08	13.31
2	0.74L, 0.78L	9.13	12.20
3	0.54L, 0.90L, 0.97L	9.33	12.22

6.2.3 Type III: Unknown source strength and location

Actual source strengths and locations versus estimated values are shown in Figure 6-4 and 6-5, respectively. Challenges that were addressed in type I and II are still present here, although for locations estimation the results are better compared to type II. Figure 6-4 reinforces the data from Figure 6-2 in which the higher the source heat input, and consequently the higher the level of turbulence, the inverse method based on Equation (4-5) struggles to estimate the source strength. While estimating source strength, an average of 5.08% error with a maximum value of 19.40% was the outcome of the inverse method with two sensors. When estimating source location, the inverse method generated results with an average error of 4.56% with a maximum value of 26.29%. Figure 6-5 proves that, like type II problems, the inverse method struggles with source locations close to the ground.

Three and four sensors scenarios were also studied. Similar to previous studies, introducing additional sensors is not affecting the accuracy of the method. Table 6-4 summarizes the output of two, three and four sensors scenarios. Overall, for the case of turbulence flow adding additional sensors is not dramatically increasing the accuracy of the method.

In application, the inverse methodology and setup should be able to respond to all three types of problems. Therefore, as type III is the most complex and general situation, it is worth discussing how the sensors that are optimal for this kind of situation would respond to type I and II problems. The results of this study are gathered in Table 6-5 and 6-6. It was expected that the results would not be as good as individual type I and II results. There are a few drastically inaccurate estimations, especially when solving for source location but overall the results are promising.

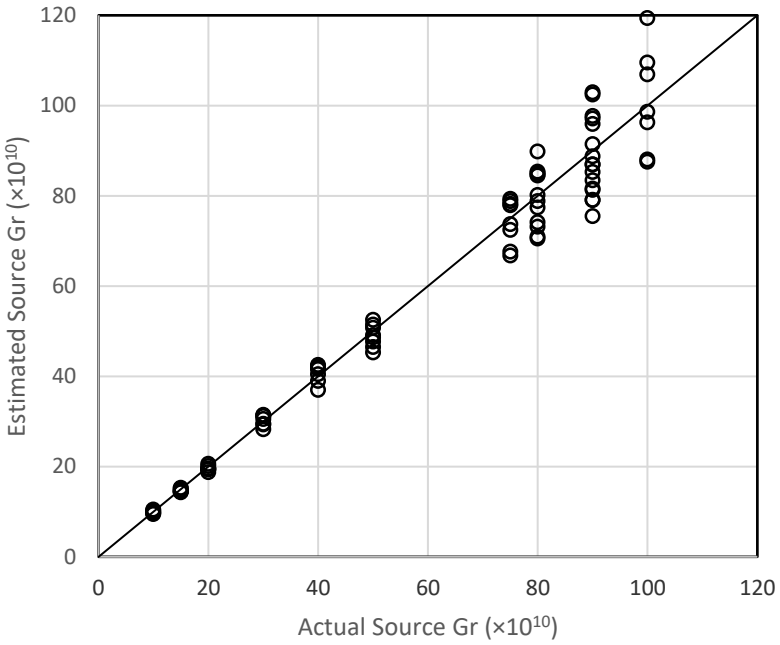

Figure 6-4- Actual vs estimated source strength using two sensors

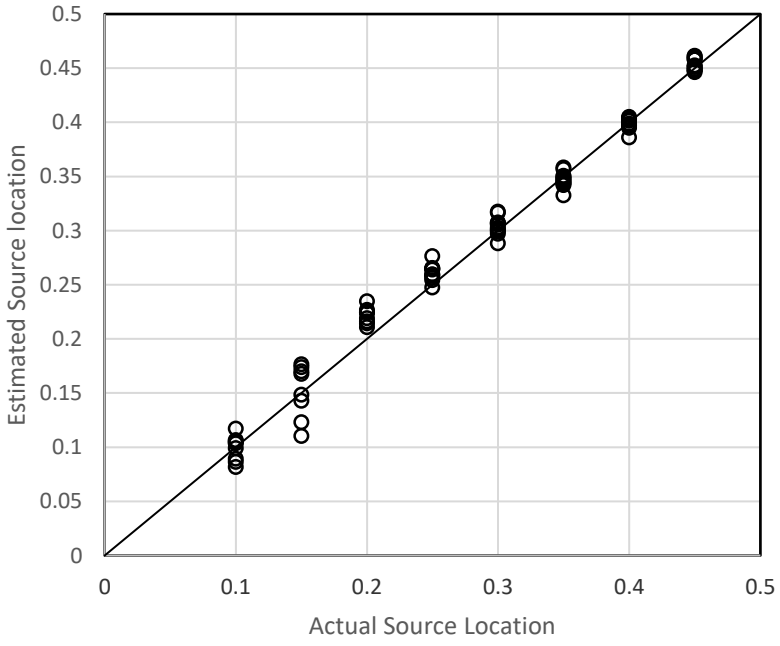

Figure 6-5- Actual vs estimated source location using two sensors

Table 6-4- Optimum sensor data – plume strength and location unknown.

Number of sensors	Location on the wall	Average % Error - *l*	Standard Deviation - *l*	Average % Error - *Gr*	Standard Deviation - *Gr*
2	0.6L, 0.65L	4.56	5.46	5.08	3.93
3	0.55L, 0.62L, 0.80L	3.98	5.95	5.20	3.75
4	0.54L, 0.68L, 0.80L, 0.97L	4.14	6.05	5.19	3.72

Table 6-5- Type I & II results using type III optimized three sensor

Type	Average % Error	Maximum % Error	Standard Deviation
I	6.29	15.37	3.78
II	8.15	77.85	14.04

Table 6-6- Type I & II estimation errors using type III optimized three sensors from sample cases.

$Gr \times 10^{10}$		30	50	80	90
l					
0.15	Gr	1.79%	0.75%	4.06%	5.14%
	l	4.45%	1.73%	8.07%	9.85%
0.25	Gr	11.43%	4.49%	2.83%	1.98%
	l	9.66%	3.72%	2.19%	1.52%
0.35	Gr	5.25%	3.67%	6.08%	7.30%
	l	2.57%	1.67%	2.78%	3.31%
0.45	Gr	12.44%	9.29%	6.80%	5.54%
	l	3.89%	2.76	1.91%	1.15%

6.3. Conclusion

In this chapter, the turbulent wall plume flow due to a heat source on the wall was studied. A $k-\omega$ model with low Reynolds corrections was used in Fluent to numerically simulate the turbulent flow. Steady-state temperatures on the wall downstream of the source were then collected and used to calculate equation (4-5) coefficients. This equation was developed earlier in chapter 4 to capture the relation between the temperatures on the wall and plume source strength and location. In order to prove its robustness, the general format of the equation was not changed, and only coefficients were updated using the turbulent temperatures. The search-based inverse methodology was then applied to the new data set.

As was expected for type I and II problems, a single sensor was enough to produce reasonable results. An average estimation error of 5.16% for the case of unknown source strength and an average of 9.08% for the unknown location was obtained. For type III, two sensors estimated the unknown source strengths and locations with an average error of 5.08% and 4.56% respectively. Increasing the number of sensors was also studied. It was observed that for all three types increasing the number of sensors did not affect the accuracy of the method. Performance of the method with type III sensors was then tested on type I and II problems and it was observed that although the results were not as refined as when using an individual type optimized sensor, the overall estimations were in an acceptable range.

Chapter 7: Inverse solution – Experiment Data

In this chapter, the inverse solution methodology that has been presented in this thesis is checked with experimental data. The experiment setup, forward results, and methodology accuracy are discussed.

7.1. Experiment apparatus

The main component of the experiment setup is a 1.5 m by 1 m by 1.5 cm piece of plywood acting as the wall. Three polyimides insulated flexible heaters (electric resistance type), 30 cm long and 2.54 cm wide each, were attached using Kapton polyimide plastic tape onto a 1 m long aluminum band. This aluminum band is 6 cm wide and 2 mm thick. Two vertical slots, 15 cm from each side of the plywood are used to move the aluminum band up and down the wall so that the heat source location can be changed. An adjustable variable transformer provides the electric current through the heaters so that the heat input can be changed. Figure 7-1 shows a schematic of the apparatus.

A total number of 8 k-type thermocouples were used to monitor the temperature along and around the plywood. A LabView card was used to capture the readings of the thermocouples. The wall plume flow, being a natural convection one, is weak in momentum and as a result susceptible to any disturbance, specifically in the form of surface irregularities caused by a thermocouple. Instead of disturbing the flow by putting thermocouples on the surface of the plywood, holes were drilled from the back of the wood and 5 thermocouples were installed inside the wall as seen in Figure 7-2. Temperature readings were then adjusted to the surface temperature values. The basic of this adjustment

lies with the main assumption that due to large aspect ratio (1.5 m : 1.5 cm) the heat conduction through the plywood can be assumed one-dimensional. Under the one-dimensional assumption, the temperature profile inside the plywood is linear as shown by equation (7-1).

$$\nabla^2 T = 0 \Rightarrow \frac{\partial^2 T}{\partial x^2} = 0 \Rightarrow T(x) = Ax + B \tag{7-1}$$

where A and B are constants. A single thermocouple was placed on the backside of the plywood on the exact location of the bottom thermocouple. Using the temperature reading from these two thermocouples, the unknown coefficients of equation (7-1) can be found. The same function is used to adjust the temperature readings of the other 4 thermocouples.

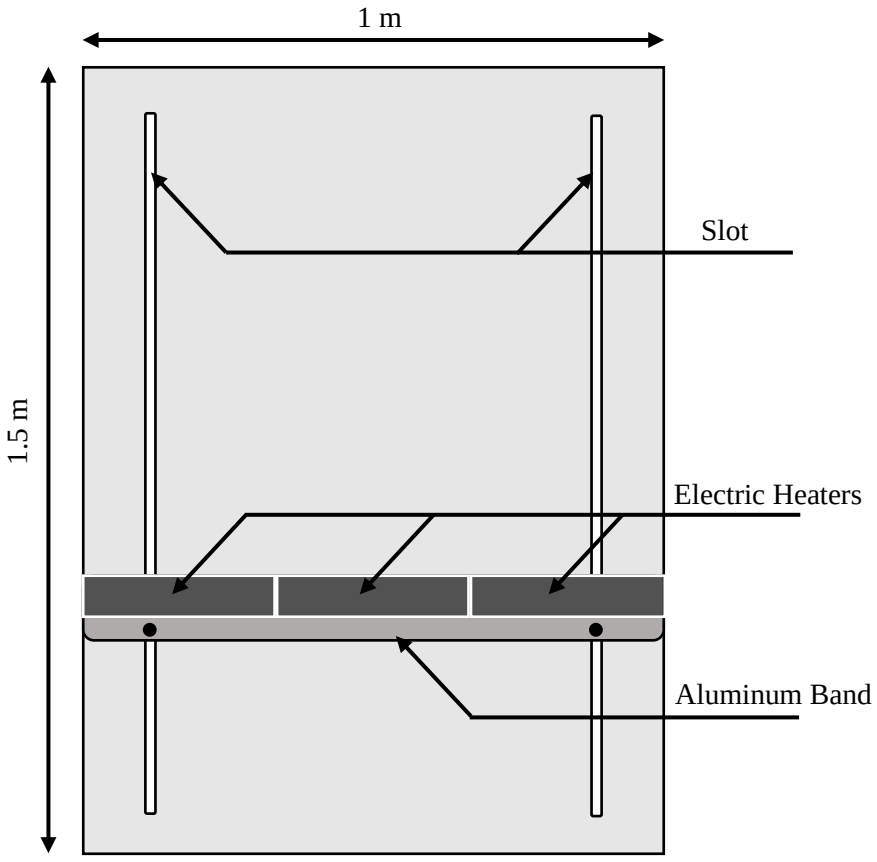

Figure 7-1- Schematic of the experiment apparatus

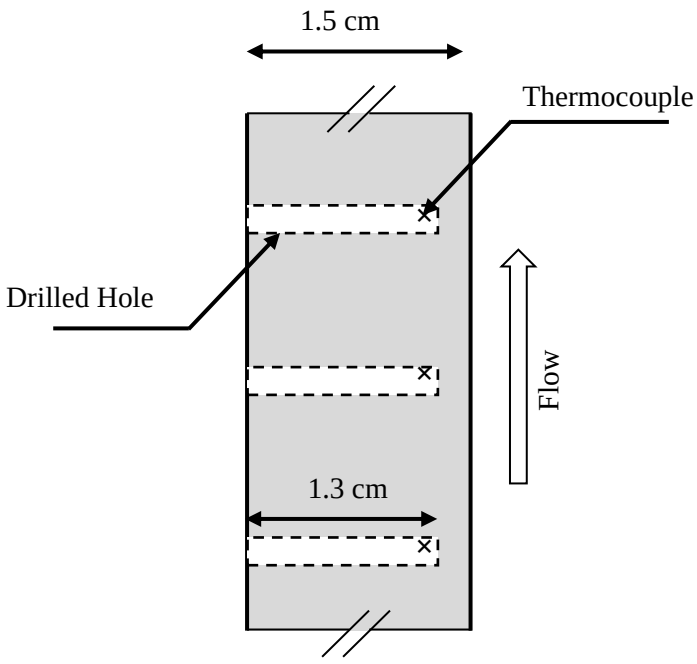

Figure 7-2- Side view of the plywood and thermocouples locations inside

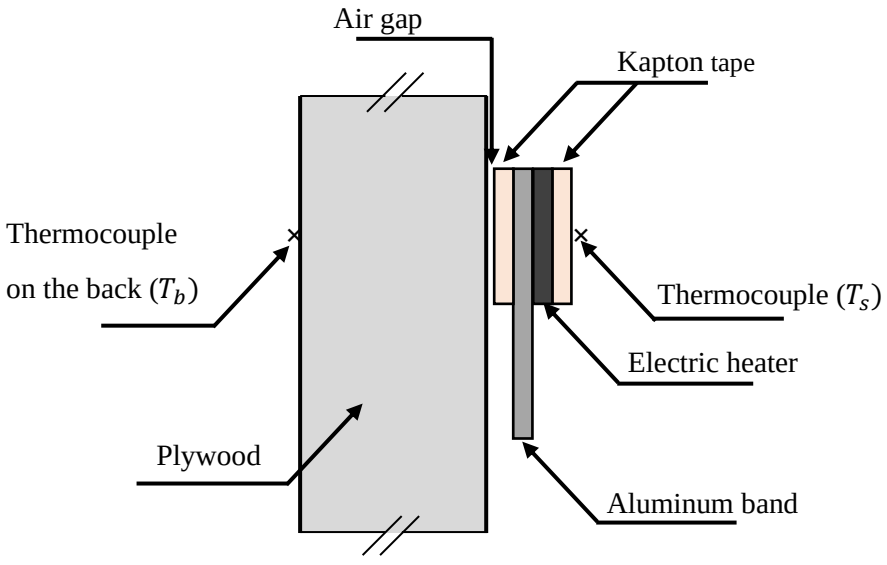

Figure 7-3- Detail of the convection calculation model

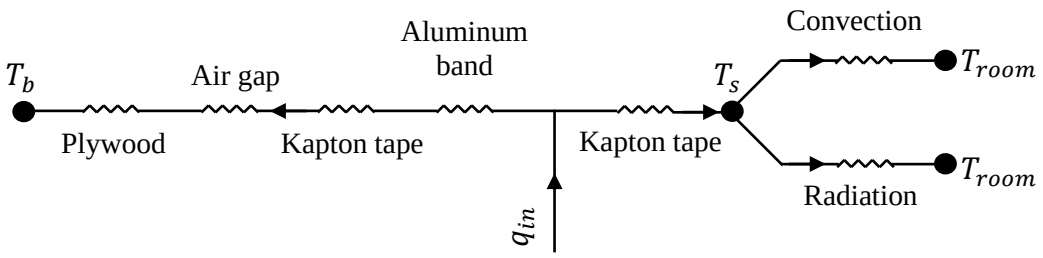

Figure 7-4- Thermal resistance schematic of the convection calculation model

The other two thermocouples are used to monitor the heater temperature. The heat input can be calculated by the power consumption of the electric heaters; however, the heater surface temperature is also required. Out of the heater total electric power input, only a portion is dissipated into natural convection. The rest of the power input goes to conduction through the plywood and radiation. In order to find how much power goes to convection, a model was developed. Figure 7-4 shows the thermal resistance representation of this model. The thermocouple was attached to the surface of the heater using a thin layer of Kapton tape.

Total electric power input is controlled by the voltage through the variable transformer. The electric resistance of each polyimide heater was measured using an ohmmeter. Power input, q_{in}, can be calculated using equation (7-2).

$$q_{in} = \frac{V^2}{R} \tag{7-2}$$

$$q''_{in} = \frac{q_{in}}{Area_{Heater}} \tag{7-3}$$

where V is voltage and R is the electric resistance. Equation (7-3) provides the input electric heat flux by dividing the input electric power over the area of the heater. Equation (7-2) calculates how much of the input power goes into convection using the heat resistance model of Figure 7-4. Input electric heat flux was calculated by

$$q''_{convection} = \frac{\left(\left(q''_{in} + \frac{T_b R_{Kap} + T_1 R_{sum}}{R_{kap} R_{sum}}\right)\frac{R_{kap} R_{sum}}{R_{kap} + R_{sum}}\right) - T_s}{R_{kap}} - \varepsilon\sigma(T_s^4 - T_{room}^4) \tag{7-4}$$

where T_s is the temperature on the heater surface, T_b is the temperature on the backside of the plywood, ε is the emissivity of the Kapton polyimide tape, σ is Stefan-Boltzmann constant and R is the heat conduction resistance calculated by equation (7-5) for each material.

$$R = \frac{L}{k} \tag{7-5}$$

where L is the thickness of the material and k is the thermal conductivity. R_{sum} in equation (7-4) is the sum of all conduction resistances between the heater surface and the backside of the plywood.

$$R_{sum} = R_{Aluminum\ band} + R_{kap} + R_{air\ gap} + R_{plywood} \tag{7-6}$$

The Grashof number can be calculated using the $q''_{convection}$ calculated from (7-4). Table 7-1 shows the calculation results using the correction equation (7-3). The heat loss to conduction and radiation are about 41% for the weakest electric input and gradually take up to approximately 48% of input energy on the highest input voltage. As the heater surface temperature increases with higher input voltages, the radiation heat loss portion gets larger than conduction heat loss because radiation is related to T_s^4.

Table 7-1- Average calculated heat fluxes for different input voltages

Voltage (V)	q''_{in} (W/m^2)	q''_{conv} (W/m^2)	q''_{rad} (W/m^2)	q''_{cond} (W/m^2)
10	120	70	30	20
50	2990	1660	860	470
75	6500	3510	2140	850
100	11800	6185	4385	1230

7.2. Results

Using the variable transformer to control the voltage of the electric heaters and the slots to move the aluminum band up and down the plywood, few different combinations of plume source strength and location were studied. Table 7-2 demonstrates the heater location on the plywood and input electric power and its corresponding Gr number for each case.

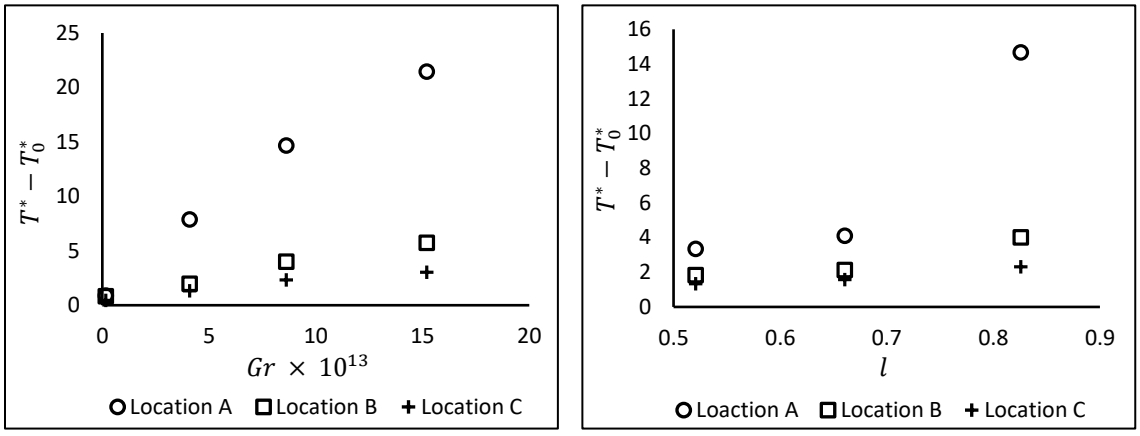

a) b)

Figure 7-5- Variation of temperature with respect to (a) source strength (l= 0.8255 m), (b) source location (Gr = 8.612× 10^{13}) - locations A, B and C represent 0.5L, 0.75L and L on the wall

Due to large proportions of the plywood, even low voltage inputs would generate a turbulent flow. Figure 7-5a and b demonstrate the temperature readings with respect to fixed source location and fixed heat input, respectively. It is observed that temperature trends are very similar in nature to those plotted in Figure 4-2c and d for laminar flow. Therefore, reinforcing the decision made in chapter 6, equation (4-5) which was initially developed for laminar flows, was used to solve the inverse problem. Only the coefficients were recalculated using the experiment temperature readings.

For the first study, 5 k-type thermocouples were placed inside the plywood at 18.75 cm spaces starting from the middle of the board and ending on top. Like the simulations in previous chapters, the thermocouples are only placed on the upper half of the wall. These thermocouples are not necessarily placed on the optimum locations; however, they still produce reasonable inverse results. Figure 7-6 shows the inverse results obtained by the temperature readings of thermocouples at 93.75 cm and 148.75 cm from the bottom of the board. These sensors provide an average error of 8.54% when estimating the plume source location and 16.26% error when estimating the source strength. The high error in strength estimation follows the trend observed in chapter 6 where equation (4-5) had difficulty predicting flows in higher turbulence regimes. When cross-checking Figure 7-6 with Table 7-2 it is observed that these sensors generally estimated better when they were closer to the plume source. This behavior was also expected based on the findings of chapter 6.

As mentioned above, the thermocouples arrangement on the plywood for the results shown in Figure 7-6 was sequential in the form of equal space in between. However, in Chapter 6, while studying the turbulent flow, an optimum location to put two sensors or thermocouples was found. Referring to Table 6-4, the optimum locations are 0.6L and

0.65L respectively on the wall. In order to check the validity of these findings, two thermocouples were replaced to 0.91 and 0.99 m on the plywood. Four sample cases were run again with the new thermocouple arrangements. Figure 7-7 shows the drastic reduction of estimation error for cases B, C, E and F when the optimum thermocouples are used. For case B, for example, the source strength estimation error has reduced from 34.77% to 1.4%. while locations estimation error is improved from 14.4% to 2.41%.

Table 7-2- Experiment cases detail

Case	Voltage (V)	$l\ (m)$	$Gr \times 10^{13}$	Case	Voltage (V)	$l\ (m)$	$Gr \times 10^{13}$
A	10	0.52	0.16	F	75	0.66	8.61
B	50	0.52	4.08	G	10	0.82	0.16
C	75	0.52	8.61	H	50	0.82	4.08
D	10	0.66	0.16	I	75	0.82	8.61
E	50	0.66	4.08	J	100	0.82	15.19

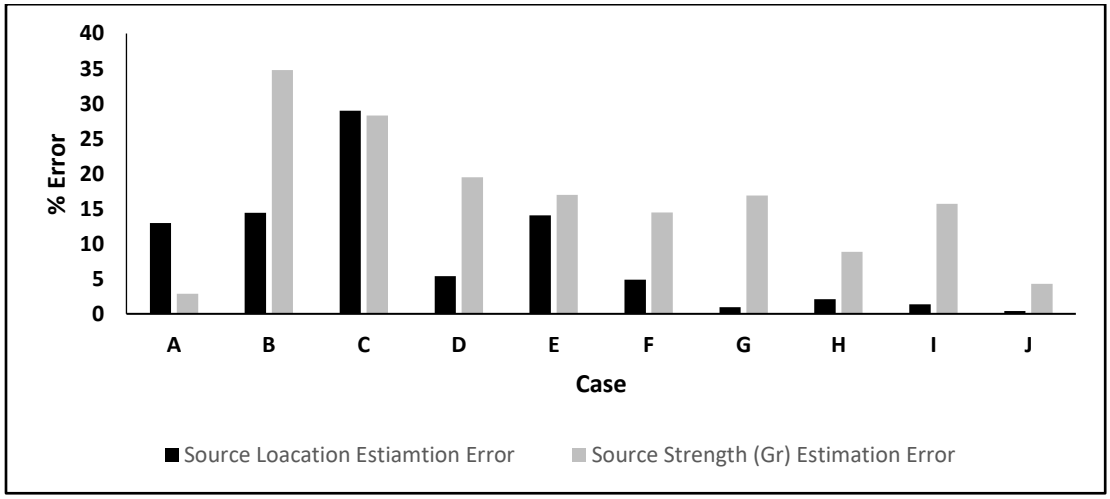

Figure 7-6- Experiment inverse results using two random sensors

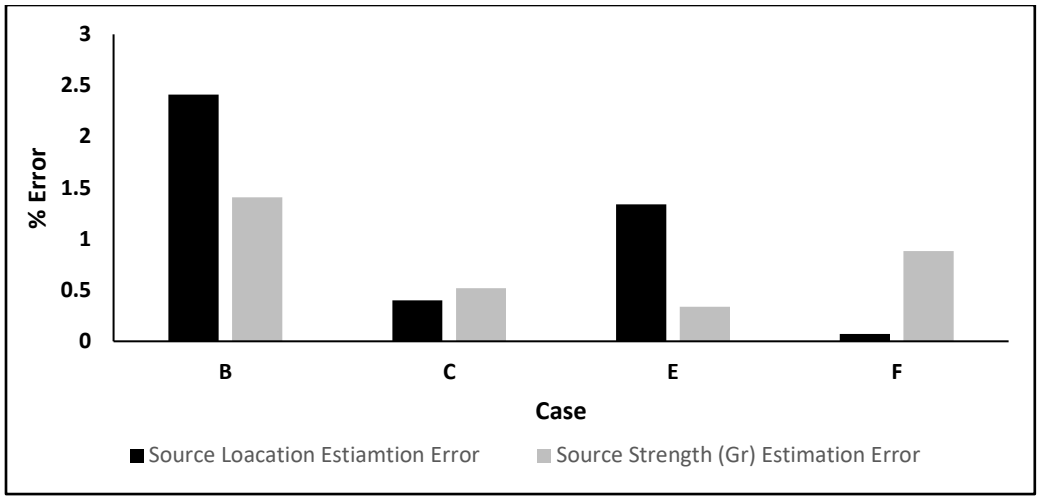

Figure 7-7- Experiment inverse results for select cases using optimum thermocouple locations

7.3. Conclusion

In this chapter, an experiment apparatus capable of producing wall plume flows with different source strengths and locations was presented. The input electric input was corrected to take heat conduction and radiation into account.

10 different combinations of wall plumes were tested. Temperature readings from 5 thermocouples placed in equal distances were then analyzed and inverse methodology was tested using equation (4-5). Similar to chapter 6, equation (4-5) provided acceptable results with the experiment turbulent flow data, even though the thermocouple arrangement was not following the optimal locations found in chapter 6. When tested against the optimal thermocouple arrangement, the method showed high accuracy in estimating both source strength and location. This experiment proves that the methodology developed throughout this thesis is capable of producing fast and reliable results within an acceptable range of accuracy for inverse natural heat convection problems.

Chapter 8: Conclusion

In this thesis, an inverse methodology based on training data sets was developed to solve a wall plume inverse heat convection problem. The methodology was tested against laminar and turbulent steady-state temperatures and transient data from numerical simulations. Finally, it was tested against experimental data and provided good accuracy through all of the said problems.

8.1. Summary of the Thesis

The proposed inverse methodology contains a study of the forward problem data to find relatable functions between various flow parameters and plume heat input and location and then using these equations to tackle the inverse problem. The laminar and turbulent steady-state temperature on the wall and transient temperature behaviors were studied numerically and a few interesting observations were made. These observations then led to different relatable functions that were then used to find unique inverse solutions.

The main challenge of this study was to find unique inverse solutions within an acceptable error range by using limited data. In order to make the proposed solutions more practical, data acquiring points were limited to the wall surface only.

Chapters 1 and 2 provide an introduction and summary to inverse heat transfer problems as well as forward transient wall plume studies. Chapter 3 goes into detail with the method and also introduces PSO as the optimization algorithm used with the methodology.

In chapter 4, the unique solution was built with steady-state temperature data only. Temperature trends were studied with respect to plume source strength, in the form of Gr, and source location. A few equations were considered to relate the features and one was selected. This equation is unique for any point downstream of the source on the wall. Through non-linear regression methods, the coefficients of this equation were determined at each point. In theory, if two of the aforementioned equations form a system of equations, one can solve the system to obtain the unknown source strength and location. In order to find the best sensor locations, PSO was used. Using the equations and a proposed objective function, PSO was able to find the best pair of sensors that would estimate the plume source strength and location with the least error. Other scenarios where only either source location or strength is unknown were also studied.

In chapter 5 transient phase of the forward flow was studied in order to find relatable functions that would connect plume source strength and location to temperature trends downstream of the plume. One of the studied flow transient features was Peak Temperature Time (PTT). Using non-linear regression methods, PTT was related to plume source strength and location in the form of a simple equation. This equation, just like the first approach, has unique coefficients at each point downstream of the plume. PSO was used again to find the best sensor locations. The effect of increasing the number of data points or sensors was also studied and it was shown that generally with an increase in the number of data points, the accuracy of the method is improved.

Chapter 6 covers the turbulent flow. Because turbulent flow is generally more complicated than a laminar one, the transient approach was put aside, and all focus was diverted to steady-state temperatures on the wall. Using the already established relatable function from

the laminar regime, the inverse methodology was applied with good accuracy. Although the equation was tailored for laminar flow initially, it adapted nicely to turbulent data and provided accurate results. It was observed that as the flow turbulence gets stronger, estimation accuracy, especially for source strength, was reduced. It was also shown that increasing the number of sensors would not affect the accuracy of the estimations dramatically.

An experiment setup was introduced in chapter 7 to test and verify the robustness of the developed methodology. All the plume flows tested were turbulent and just chapter 6, the same relatable equation from chapter 4 was tested. The results showed good accuracy, especially when estimating the plume location. When the optimal thermocouple locations from chapter 6 were tested with the experiment data, a high level of accuracy was achieved.

8.2. Future Work

There is room to improve this methodology. One possibility is to study other transient features such as peak temperature or the temperature rise initiation time and integrate them into the solution method. Also combining the results of transient and steady-state results could increase the overall accuracy, reduce the uncertainty of the solutions and help to reach unique solutions. Transient inverse results could act as first estimations while steady-state inverse results could fine-tune the transient solutions.

Machine learning and deep learning have gained momentum, especially in the last decade thanks to the ever-increasing computational power of modern computer systems. They have gradually gained a foothold in other science disciplines from health care [69-71] to fluid mechanics [72-74]. These techniques usually require a big data set to train the

algorithm, however, with the power of computers today, it is a relevantly straight forward process to numerically mass simulate forward problems with different boundary conditions and feed the algorithm. This is a promising front for mechanical engineering and fluid mechanics in general and inverse heat transfer problems in particular. Instead of finding the relative functions by human study, the computer would use the huge training data set to regulate complex relations between multiple problem parameters at once and produce accurate results.

The ultimate goal of this study is to find solutions to small fires or overheating electric devices in rooms. To that end, trying more complex geometries such as cavities with and without openings would be the next step. However, this has proven to be more challenging than it seems. A considerable amount of work during this project was dedicated to solving the inverse heat transfer problem in cavities with openings. The results of the forward problem were promising but hard to analyze with the inverse solution in mind. Here is where the machine or deep learning algorithms could shine. Providing the algorithm with a considerable amount of raw data in the form of transient and steady-state fluid temperature and velocity inside the cavity for different heat source locations and strengths to form up the training data set would be the first step. The focus of this proposed research should be on tuning a suitable algorithm to find unique inverse solutions within an acceptable range of accuracy.

Bibliography

1. Hadamard, J., *Lectures on Cauchy's problem in linear partial differential equations*. 2003: Courier Corporation.
2. Beck, J., *Blackwell and CR St. Clair, Jr., Inverse Heat Conduction: Ill-Posed Problems*. 1985, New York: John Wiley and Sons.
3. Orlande, H.R., et al., *Thermal measurements and inverse techniques*. 2011: CRC Press.
4. Ozisik, M.N., *Inverse heat transfer: fundamentals and applications*. 2000: CRC Press.
5. Tikhonov, A.N. and V.I. Arsenin, *Solutions of ill-posed problems*. Vol. 14. 1977: Winston, Washington, DC.
6. Alifanov, O., *Solution of an inverse problem of heat conduction by iteration methods.* Journal of engineering Physics and Thermophysics, 1974. **26**(4): p. 471-476.
7. Alifanov, O.M., *Inverse heat transfer problems*. 2012: Springer Science & Business Media.
8. Alifanov, O. and A. OM, *DETERMINATION OF THERMAL LOADS FROM THE SOLUTION OF NON-LINEAR INVERSE PROBLEM.* 1977.
9. Beck, J.V. and K.J. Arnold, *Parameter estimation in engineering and science*. 1977: James Beck.
10. Monde, M., et al., *An analytical solution for two-dimensional inverse heat conduction problems using Laplace transform.* International Journal of Heat and Mass Transfer, 2003. **46**(12): p. 2135-2148.
11. Tian, N., L. Zhu, and C.-H. Lai, *Estimation of heat transfer coefficient in inverse heat conduction problem using quantum-behaved particle swarm optimization with Tikhonov regularization.* Journal of Algorithms & Computational Technology, 2014. **8**(2): p. 233-248.
12. Huang, C. and M. Özisik, *Inverse problem of determining unknown wall heat flux in laminar flow through a parallel plate duct.* Numerical Heat Transfer, 1992. **21**(1): p. 55-70.
13. Liu, F. and M. Ozisik, *Inverse analysis of transient turbulent forced convection inside parallelplate ducts.* International journal of heat and mass transfer, 1996. **39**(12): p. 2615-2618.
14. Hsu, P.-T., C.o.-K. Chen, and Y.-T. Yang, *A 2-D inverse method for simultaneous estimation of the inlet temperature and wall heat flux in a laminar circular duct flow*. Numerical Heat Transfer, Part A Applications, 1998. **34**(7): p. 731-745.
15. Knight, D., et al. *Evaluation of fluid-thermal systems by dynamic data driven application systems-part ii*. in *International Conference on Computational Science*. 2007. Springer.
16. VanderVeer, J.R. and Y. Jaluria, *Solution of an inverse convection problem by a predictor–corrector approach.* International Journal of Heat and Mass Transfer, 2013. **65**: p. 123-130.
17. VanderVeer, J.R. and Y. Jaluria, *Optimization of an inverse convection solution strategy.* International Journal of Heat and Mass Transfer, 2014. **73**: p. 664-670.

18. VanderVeer, J.R. and Y. Jaluria, *Solution of the inverse jet in a crossflow problem by a predictor–corrector technique*. International Journal of Heat and Mass Transfer, 2015. **89**: p. 929-936.
19. Bangian-Tabrizi, A. and Y. Jaluria, *An optimization strategy for the inverse solution of a convection heat transfer problem.* International Journal of Heat and Mass Transfer, 2018. **124**: p. 1147-1155.
20. Scott, E.P., *Inverse Heat Transfer for Biomedical Applications.* Theory and Applications of Heat Transfer in Humans, 2018. **1**: p. 133-152.
21. Prud'homme, M. and T.H. Nguyen, *Solution of inverse free convection problems by conjugate gradient method: effects of Rayleigh number.* International journal of heat and mass transfer, 2001. **44**(11): p. 2011-2027.
22. Park, H. and O. Chung, *An inverse natural convection problem of estimating the strength of a heat source.* International journal of heat and mass transfer, 1999. **42**(23): p. 4259-4273.
23. Bangian-Tabrizi, A. and Y. Jaluria, *A study of transient wall plume and its application in the solution of inverse problems.* Numerical Heat Transfer, Part A: Applications, 2019. **75**(3): p. 149-166.
24. Bergman, T.L., et al., *Fundamentals of heat and mass transfer*. 2011: John Wiley & Sons.
25. Cengel, A., *HEHT TRANSFER.* 2003.
26. Lin, W., S. Armfield, and J. Patterson, *Unsteady natural convection boundary-layer flow of a linearly-stratified fluid with Pr< 1 on an evenly heated semi-infinite vertical plate.* International Journal of Heat and Mass Transfer, 2008. **51**(1-2): p. 327-343.
27. Ostrach, S., *An analysis of laminar free-convection flow and heat transfer about a flat plate parallel to the direction of the generating body force*. 1952, NATIONAL AERONAUTICS AND SPACE ADMINISTRATION CLEVELAND OH LEWIS RESEARCH CENTER.
28. Schmidt, E. and W. Beckmann, *Das Temperatur-und Geschwindigkeitsfeld vor einer Wärme abgebenden senkrechten Platte bei natürlicher Konvektion.* Technische Mechanik und Thermodynamik, 1930. **1**(11): p. 391-406.
29. Eckert, E. and E. Soehngen, *Studies on heat transfer in laminar free convection with the Zehnder-Mach interferometer*. 1948, AIR MATERIEL COMMAND WRIGHT-PATTERSON AFB OH.
30. Schuh, H., *Boundary layers of temperature.* Boundary Layers, 1948.
31. Gregg, E.S.J. and J. Sparrow, *Laminar Free Convection From a Vertical Plate with Uniform Surface Heat Flux.* Trams, ASME, 1956. **48**: p. 435-440.
32. Siegel, R., *Transient free convection from a vertical flat plate.* Trans. Asme, 1958. **80**(2): p. 347.
33. Hellums, J. and S.W. Churchill, *Transient and steady state, free and natural convection, numerical solutions: Part I. The isothermal, vertical plate.* AIChE Journal, 1962. **8**(5): p. 690-692.
34. Harris, S., et al., *Transient free convection flow past a vertical flat plate subject to a sudden change in surface temperature.* International journal of heat and mass transfer, 1998. **41**(2): p. 357-372.

35. Maranzana, G., et al., *Experimental estimation of the transient free convection heat transfer coefficient on a vertical flat plate in air.* International journal of heat and mass transfer, 2002. **45**(16): p. 3413-3427.
36. Eckert, E. and T.W. Jackson, *Analysis of turbulent free-convection boundary layer on flat plate*. 1950, National Aeronautics and Space Administration Washington DC.
37. Cheesewright, R., *Turbulent natural convection from a vertical plane surface.* 1968.
38. Tsuji, T. and Y. Nagano, *Characteristics of a turbulent natural convection boundary layer along a vertical flat plate.* International journal of heat and mass transfer, 1988. **31**(8): p. 1723-1734.
39. George Jr, W.K. and S.P. Capp, *A theory for natural convection turbulent boundary layers next to heated vertical surfaces.* International Journal of Heat and Mass Transfer, 1979. **22**(6): p. 813-826.
40. To, W. and J. Humphrey, *Numerical simulation of buoyant, turbulent flow—I. Free convection along a heated, vertical, flat plate.* International journal of heat and mass transfer, 1986. **29**(4): p. 573-592.
41. Nakao, K., Y. Hattori, and H. Suto, *Numerical investigation of a spatially developing turbulent natural convection boundary layer along a vertical heated plate.* International Journal of Heat and Fluid Flow, 2017. **63**: p. 128-138.
42. Rundle, C. and M. Lightstone. *Validation of turbulent natural convection in square cavity for application of CFD modelling to heat transfer and fluid flow in atria geometries*. in *2nd Canadian Solar Building Conference, Calgary, Canada*. 2007. Citeseer.
43. Gebhart, B., et al., *Buoyancy-induced flows and transport.* 1988.
44. Sugawara, S. and I. Michiyoshi. *The heat transfer by natural convection in the unsteady state on a vertical flat wall*. in *Proceedings of the First Japan National Congress for Applied Mechanics*. 1951.
45. Ahmadi, M. and M. Bahrami. *Modeling Transient/Steady-State Convection from Isoflux Vertical Plates*. in *ASME 2012 Heat Transfer Summer Conference collocated with the ASME 2012 Fluids Engineering Division Summer Meeting and the ASME 2012 10th International Conference on Nanochannels, Microchannels, and Minichannels*. 2012. American Society of Mechanical Engineers.
46. Schetz, J. and R. Eichhorn, *Unsteady natural convection in the vicinity of a doubly infinite vertical plate.* Journal of Heat Transfer, 1962. **84**(4): p. 334-338.
47. Menold, E. and K.-T. Yang, *Asymptotic solutions for unsteady laminar free convection on a vertical plate.* Journal of Applied Mechanics, 1962. **29**(1): p. 124-126.
48. Rao, A.K., *Unsteady natural convection from a vertical flat plate with suction.* Applied Scientific Research, 1961. **10**(1): p. 141.
49. Miyamoto, M., *Influence of variable properties upon transient and steady-state free convection.* International Journal of Heat and Mass Transfer, 1977. **20**: p. 1258-1261.
50. Illingworth, C. *Unsteady laminar flow of gas near an infinite flat plate*. in *Mathematical Proceedings of the Cambridge Philosophical Society*. 1950. Cambridge University Press.

51. Goldstein, R. and D. Briggs, *Transient free convection about vertical plates and circular cylinders.* Journal of Heat Transfer, 1964. **86**(4): p. 490-500.
52. Gebhart, B. and R. Dring, *The leading edge effect in transient natural convection from a vertical plate.* Journal of Heat Transfer, 1967. **89**(3): p. 274-275.
53. Mollendorf, J.C. and B. Gebhart, *An experimental study of vigorous transient natural convection.* Journal of Heat Transfer, 1970. **92**(4): p. 628-634.
54. Mahajan, R. and B. Gebhart, *Leading edge effects in transient natural convection flow adjacent to a vertical surface.* Journal of Heat Transfer, 1978. **100**(4): p. 731-733.
55. Patterson, J.C., et al., *Boundary layer development on a semi-infinite suddenly heated vertical plate.* Journal of Fluid Mechanics, 2002. **453**: p. 39-55.
56. Fujii, T., *Theory of the steady laminar natural convectiol above a horizontal line heat source and a point heat source.* International Journal of Heat and Mass Transfer, 1963. **6**(7): p. 597-606.
57. Gebhart, B., L. Pera, and A. Schorr, *Steady laminar natural convection plumes above a horizontal line heat source.* International Journal of Heat and Mass Transfer, 1970. **13**(1): p. 161-171.
58. Zimin, V. and Y.N. Lyakhov, *Convective wall plume.* Journal of Applied Mechanics and Technical Physics, 1970. **11**(3): p. 511-513.
59. Jaluria, Y., *Mixed convection in a wall plume.* Computers & Fluids, 1982. **10**(2): p. 95-104.
60. Jaluria, Y. and B. Gebhart, *Buoyancy-induced flow arising from a line thermal source on an adiabatic vertical surface.* International Journal of Heat and Mass Transfer, 1977. **20**(2): p. 153-157.
61. Colaço, M.J., H.R. Orlande, and G.S. Dulikravich, *Inverse and optimization problems in heat transfer.* Journal of the Brazilian Society of Mechanical Sciences and Engineering, 2006. **28**(1): p. 1-24.
62. Kennedy, J. *The particle swarm: social adaptation of knowledge*. in *Evolutionary Computation, 1997., IEEE International Conference on*. 1997. IEEE.
63. Eberhart, R. and J. Kennedy. *A new optimizer using particle swarm theory*. in *Micro Machine and Human Science, 1995. MHS'95., Proceedings of the Sixth International Symposium on*. 1995. IEEE.
64. Bonyadi, M.R. and Z. Michalewicz, *Particle swarm optimization for single objective continuous space problems: a review*. 2017, MIT Press.
65. Zhang, Y., S. Wang, and G. Ji, *A comprehensive survey on particle swarm optimization algorithm and its applications.* Mathematical Problems in Engineering, 2015. **2015**.
66. Moré, J.J., *The Levenberg-Marquardt algorithm: implementation and theory*, in *Numerical analysis*. 1978, Springer. p. 105-116.
67. Wilcox, D.C., *Reassessment of the scale-determining equation for advanced turbulence models.* AIAA journal, 1988. **26**(11): p. 1299-1310.
68. Henkes, R. and C. Hoogendoorn, *Comparison exercise for computations of turbulent natural convection in enclosures.* Numerical Heat Transfer, Part B Fundamentals, 1995. **28**(1): p. 59-78.

69. Mehrizi, R., et al. *Toward marker-free 3D pose estimation in lifting: A deep multi-view solution*. in *2018 13th IEEE International Conference on Automatic Face & Gesture Recognition (FG 2018)*. 2018. IEEE.
70. Mehrizi, R., et al., *A Deep Neural Network-based method for estimation of 3D lifting motions.* Journal of biomechanics, 2019. **84**: p. 87-93.
71. Mehrizi, R., et al., *A computer vision based method for 3D posture estimation of symmetrical lifting.* Journal of biomechanics, 2018. **69**: p. 40-46.
72. Raissi, M., et al., *Deep learning of vortex-induced vibrations.* Journal of Fluid Mechanics, 2019. **861**: p. 119-137.
73. Wang, Z., et al., *Model identification of reduced order fluid dynamics systems using deep learning.* International Journal for Numerical Methods in Fluids, 2018. **86**(4): p. 255-268.
74. Raissi, M., A. Yazdani, and G.E. Karniadakis, *Hidden fluid mechanics: A navier-stokes informed deep learning framework for assimilating flow visualization data.* arXiv preprint arXiv:1808.04327, 2018.